Review of aeronautical fatigue and structural integrity investigations in the Netherlands during the period March 2017 - March 2019

TU Delft

Review of aeronautical fatigue and structural integrity investigations in the Netherlands during the period March 2017 - March 2019

R.C. Alderliesten

Abstract

This report is a review of the aeronautical fatigue and structural integrity activities in the Netherlands during the period March 2017 to March 2019. The review is the Netherlands National Delegate's contribution to the 36th Conference of the International Committee on Aeronautical Fatigue and Structural Integrity (ICAF) in Krakow, Poland, on 2 and 3 June 2019.

An electronic version of this review is available at **http://repository.tudelft.nl/**.

Table of Contents

Abbreviations

AE	Acoustic Emission
AM	Additive Manufacturing
CA	Constant Amplitude
CBP	Composite Bell Peel
CFRP	Carbon fibre reinforced polymer composites
CLS	Cracked Lap Shear
DAF	Disbond Arrest Feature
DCB	Double Cantilever Beam
DIC	Digital Image Correlation
EIFS	Equivalent Initial Flaw Size
FBG	Fibre-Bragg Grating
FCG	Fatigue Crack Growth
FE	Finite Element
FML	Fibre Metal Laminate
FOS	Fibre Optic Sensing
FSW	Friction Stir Welding
GFRP	Glass fibre reinforced polymer composites
GW	Guided waves
HIP	High Isostatic Pressure
LEFM	Linear Elastic Fracture Mechanics
POF	Probability of Failure
PROF	PRrediction Of Fatigue in engineering alloys
QF	Quantitative Fractography
RNLAF	Royal Netherlands Air Force
RUL	Remaining Useful Life
SERR	Strain Energy Release Rate
SHM	Structural Health Monitoring
SIF	Stress Intensity Factor
SRA	Structural Risk Analysis
TRL	Technology Readiness Level
UD	Unidirectional
UW	Ultrasonic Welding
VA	Variable Amplitude

1. Introduction

The present report provides an overview of the work and research performed in the Netherlands in the field of aeronautical fatigue and structural integrity during the period from March 2017 until March 2019. The subjects in this review come from the following contributors:

- Delft University of Technology (TU Delft)
- GKN Aerospace-Fokker (GKN Fokker)
- Netherlands Aerospace Centre (NLR)
- Royal Netherlands Air Force (RNLAF)
- University of Twente (UT)

Additionally, collaborative work between the NLR and the Defence Science and technology Group (DST-G) of Australia, and between TU Delft and various European universities and institutes is included.

The names of the principal investigators and their affiliations are provided at the start of each subject. The format and arrangement of this review is similar to that of previous national reviews.

2. Metal Fatigue

2.1. Interaction between stress ranges and stress ratios during variable amplitude

Jesse van Kuijk, René Alderliesten, TU Delft

This PhD research project focuses on the physics underlying constant and variable amplitude (VA) fatigue crack growth in relation to stress ranges and opening/closing stresses. The concepts of physics considered are the application of strain energy (work) when loading, and the dissipation of energy through plasticity and the formation crack surfaces.

The latter was initially explored through correlating the formation of crack surface area with the more common one-dimensional crack length. The main question addressed was whether the use of the crack surface area as base parameter rather than crack length would improve existing models, or at least explain certain observations reported in literature. Correlating a model based on crack area with cracks observed developing in laboratory experiments suggested indeed an improvement, which tends to indicate that crack area is a better base parameter than crack length, in particular for small cracks propagating in a planar fashion. This study was presented at the Fatigue 2018 Conference in Poitiers, France [1].

Fatigue tests on aluminium 2024-T3 CCT specimens containing through- and corner-cracks were performed to study the crack front growth post-mortem through optical and electron microscopy. The measurements of crack lengths through digital photography and the measurement of plastic crack tip fields through digital image correlation systems proved successful in capturing crack growth rate and plasticity development. Crack lengths were accurately measured with the potential drop technique, allowing measurement of the pivot points [2] in the crack growth curve.

An energy approach to crack growth is currently investigated, assessing the elastic, plastic, and crack growth energy (dissipation) components of a cracked plate undergoing constant amplitude fatigue loading, and later also VA loading. To understand how these components change with increasing crack length and time, a theoretical model is in development to explicitly describe the various energy components during one crack growth cycle. The development of this model is supported with finite element simulations, replicating the physical fatigue crack growth experiments as digital twin, to gain insight and quantitative information on the different energy components. Integrating this through-the-cycle model expressed in *d/dt* yields a crack growth rate *d/dN*, to be related to experimental data and legacy prediction models.

The role of the opening stress S_{op} in the ΔK_{eff} similitude parameter in relation to crack closure phenomena has been studied with finite element analyses and theoretical modelling. A new physical model based on the cyclic energy per half cycle is proposed (schematically illustrated in Figure 1). This study will soon be published.

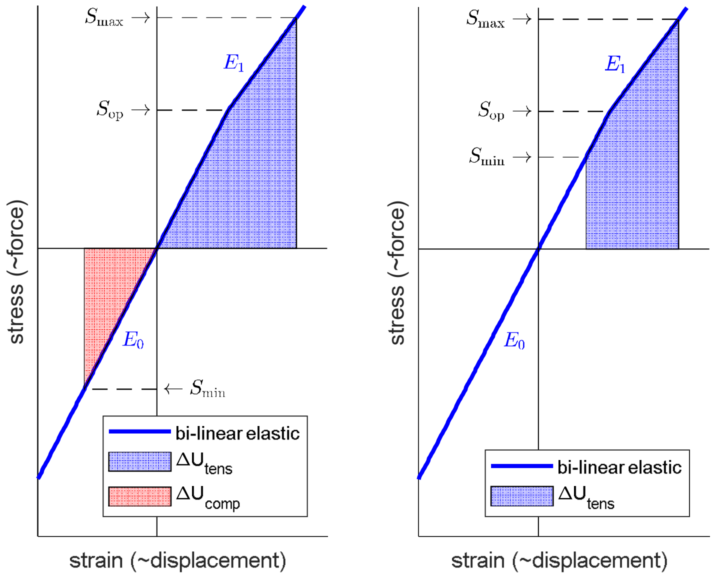

Figure 1 The change in energy during a loading cycle, for two different R values, for a bi-linear elastic material. When the crack opens, the stiffness changes. The sum of the area under the curve for each case is equal to the applied cyclic energy in that specific cycle.

2.2. Prediction of fatigue in engineering alloys (PROF)

Emiel Amsterdam, Netherlands Aerospace Centre NLR

The objective of the project “Prediction of fatigue in engineering alloys (PROF)” is to improve the physical understanding and prediction of fatigue in engineering alloys. This four year project was initiated by NLR in 2016, in collaboration with Fokker, Embraer, Airbus Lloyd’s Register and Wärtsilä. Delft University of Technology and the Royal Netherlands Air Force are also involved in the project.

In the project it is clearly demonstrated that crack growth in AA7075-T7351 shows a power law relationship with ΔK at all tested length scales/ΔK values. The power law behaviour at all crack lengths, the introduction of pivot points and modern computer technology allow fitting of the a-N curve to obtain crack growth rates without any noise. This replaces the method of incremental polynomial fitting, which introduces noise and errors in the crack growth rate results. The ability to obtain very accurate crack growth rates will require less testing in the future and opens up a whole range of opportunities for understanding crack growth in ductile materials. It can also be used, for example, to exactly determine the influence of small factors such as temperature, humidity and frequency. Fatigue crack growth during VA testing also exhibits power law behaviour between pivot points. The crack growth is exponential at higher stress intensity factors (SIF), where the SIF is calculated with the maximum stress of the VA spectrum. At lower SIF values the power law exponents are greater than for the exponential crack growth region (where the exponent equals two). The measurements show that the crack growth rate has a power law relationship with the SIF for different maximum stresses.
Some of the results have already been published [3,4].

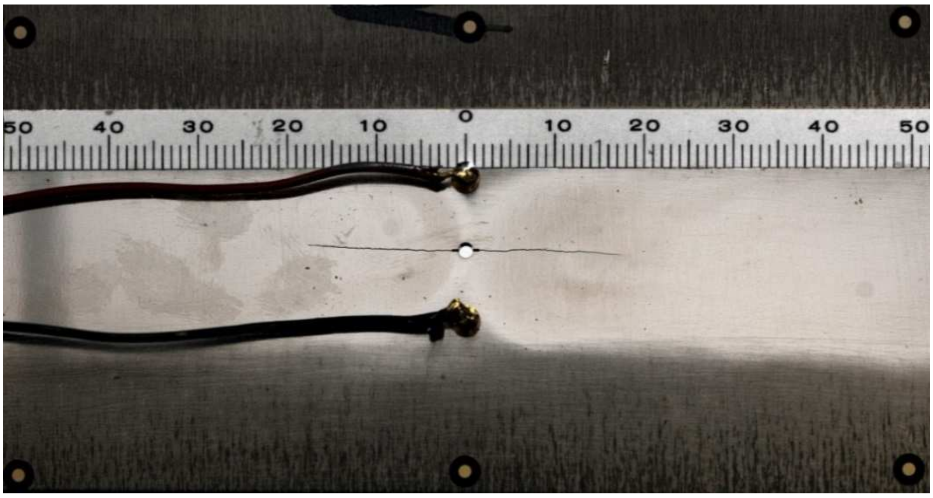

Figure 2 Aluminium 7075-T7351 coupon with a fatigue crack. The crack size is measured both optically and with the direct current potential drop (DCPD) technology.

2.3. On the plastic dissipation during fatigue crack growth

Hongwei Quan, René Alderliesten, TU Delft

Although Linear Elastic Fracture Mechanics (LEFM) has been applied successfully to practical engineering fatigue problems through the use of the Paris relation, it does not take into account explicitly the plasticity phenomena that strongly influence fatigue crack growth rates (*da/dN*). In this study, the fatigue crack phenomena were studied from a physical perspective. An energy approach was chosen because its universality for various materials, and because plasticity itself represents an important type of energy dissipation for metallic materials.

Some literature [5] proposes a linear relation between the total plastic dissipation per cycle (dU_{pl}/dN) and fatigue crack growth rate (*da/dN*), and also claims that the value of the plastic dissipation per unit fatigue crack growth (dU_{pl}/da) constitutes a material property that is nearly constant. In order to verify such relationship, fatigue crack growth experiments were performed.

These fatigue experiments were performed force-controlled on central crack tension (CCT) fatigue crack growth specimens made of 2024-T3. The test set-up is shown in the left-hand side of Figure 3. The fatigue crack length was measured by visual observation, while the energy dissipation per cycle was obtained through load and displacement measurements on the specimens. The load values were recorded by the fatigue test machine, while the displacement was measured were performed using DIC. More information is presented in [6].

From the fatigue experiments, it could be concluded that the plastic energy dissipation (dU_{pl}/dN) shows a nonlinear relation with *da/dN*, as illustrated in the right-hand side of Figure 3. Thus the value of dU_{pl}/da is not constant throughout the test. Therefore, the plastic energy dissipation cannot be used to predict *da/dN* directly.

The reason is that the dU_{pl}/dN is not an effective similitude parameter. From a physical perspective, the energy balance equation of fatigue crack growth could be described as:

$$\frac{dW}{dN} = \frac{dU_a}{dN} + \frac{dU_{pl}}{dN} + \frac{dU_e}{dN}$$

The physical meaning of this equation is that the total dissipated energy (work) during one cycle *dW/dN* is the sum of the energy dissipation for the new fatigue crack surface formation dU_a/dN the plastic dissipation during one cycle dU_{pl}/dN and the elastic strain energy change after one cycle dU_e/dN. The fatigue crack propagation is only directly related to dU_a/dN, while dU_{pl}/dN and dU_e/dN are consequences of the fatigue crack growth.

Theoretically, the crack surface forming energy is the proper similitude parameter that is directly linked to fatigue crack growth, instead of the plastic energy dissipation. However, the value of dU_a/dN is too small to be measured accurately in reality. Therefore, the dU_{pl}/dN seems to be the only option left for that its value can be obtained. However, based on the current study one should be aware that plastic dissipation and fatigue crack growth are not directly related, and some extra efforts are needed to link these quantities.

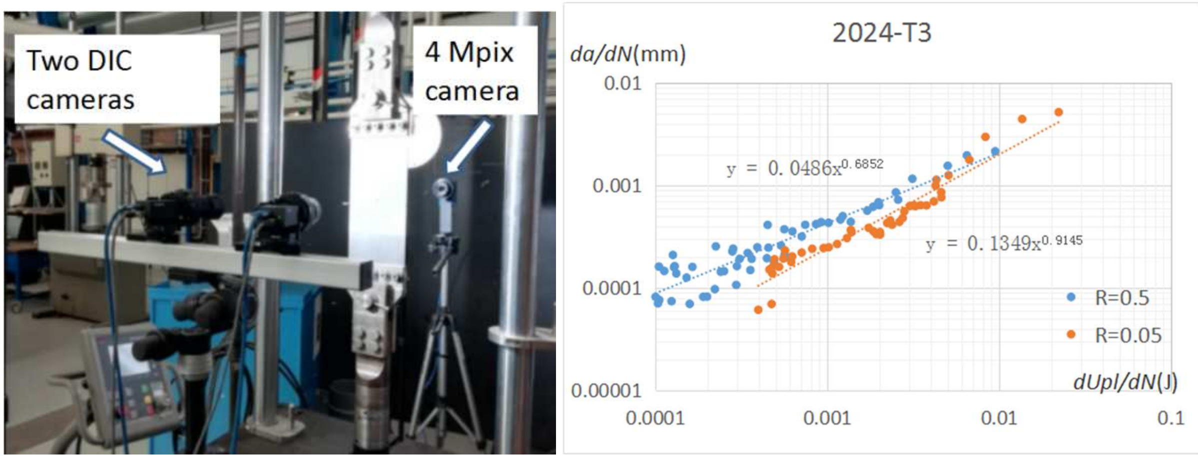

Figure 3 The set-up of the experiments [6] (left), and the total plastic dissipation versus fatigue crack growth rate (right)

2.4. Stress-life properties of laser powder bed fusion Inconel 718 fatigue specimens

Emiel Amsterdam and Gerrit Kool, Netherlands Aerospace Centre NLR

The objective of this program was to obtain statistical information on the stress life of additively manufactured (‘3D-printed’) Inconel 718 at a given maximum stress level. The distribution of the number of cycles to failure gives information on the material properties and the defect distribution inside the specimens. The specimens were machined and polished to obtain the bulk material stress life properties and exclude influences from surface roughness. Tensile static and fatigue specimens were printed by laser powder bed fusion (L-PBF) with different settings, because the mechanical properties and defect distribution can vary with build parameters, location & orientation and post processing. The specimens were printed in several orientations with respect to the build direction; horizontal, vertical and at 45° inclination with the build plate – see Figure 4. Powder layer thicknesses of 30 and 50 µm were used. A fraction of the specimens received a hot isostatic pressing (HIP) treatment prior to the conventional heat treatment, to obtain information on the effect of the HIP treatment on the defect distribution of the material. The results were compared with results from fatigue tests on IN718 plate material that received a similar heat treatment. The results showed a significant higher stress life for the printed material in all three orientations compared to the fatigue tests on IN718 plate material and results from literature, despite the presence of typical L-PBF defects such as porosity. Fractography and microstructural analysis indicated that the higher stress life originates from a particular microstructure, which resulted in a different short crack behaviour – see Figure 5. Even though the grain structure was changed after the HIP treatment, the L-PBF specific microstructure was partly retained, which resulted in a stress life between conventional heat treated L-PBF material and plate material.

Figure 4 The 3D-printed Inconel 718 specimens.

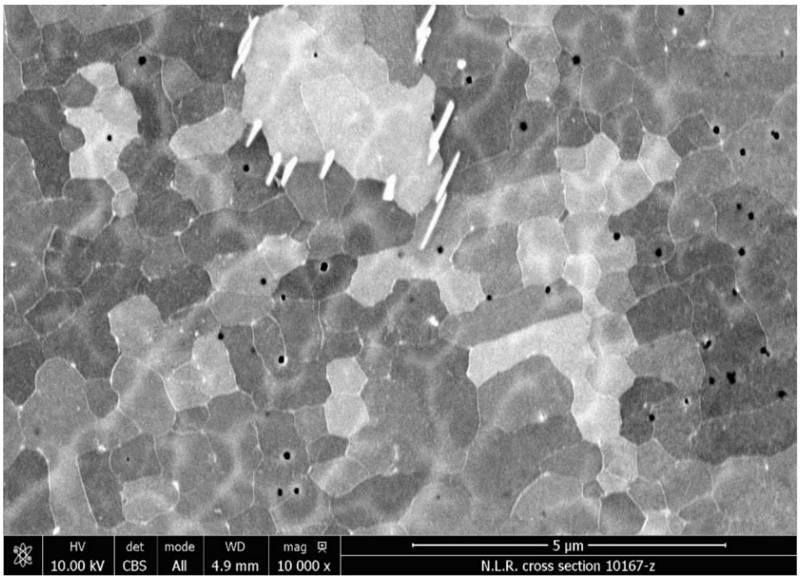

Figure 5 SEM images of the microstructure, showing subgrains.

2.5. Additive Manufacturing and Certification of Flight Critical part

H.N. Kamphuis, M. Bosman, Tim Janssen (GKN Fokker), Calvin Rans (TU Delft), M. van Hintem (MOD), G.A. Kool (NLR)

Additive Manufacturing (AM) is a manufacturing process where parts are built layer by layer to form a complex 3D shape. Compared to conventional subtractive manufacturing technologies it offers benefits in design freedom and material usage, making it very useful for expensive hard metals like titanium. Currently AM technology has found its first applications in aircraft at non- flight critical parts at low rate production. Since the AM process is still emerging towards industrial standards, the use of AM parts is still very limited and not yet ready for critical applications. There is a need for more proof to build confidence that the new AM technologies are robust and reliable enough to be widely used in aerospace. Also the huge potential AM offers to reduce weight and improve performance by complex, bionic designs for functional parts is starting to be exploited now. This will be the logical next step after AM technology has been accepted by industry and airworthiness authorities.

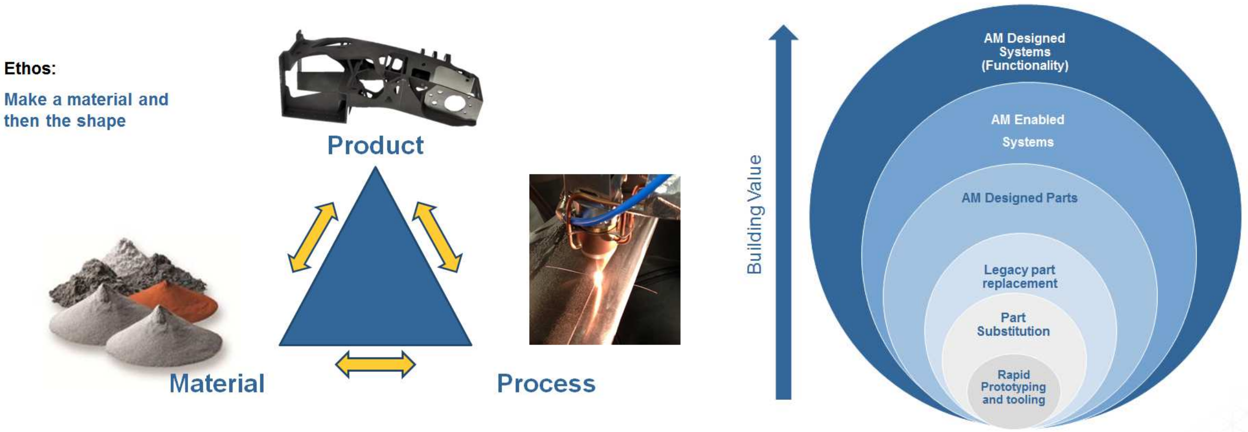

Figure 6 From material to shape with Additive Manufacturing (AM) (left), and Value increase of AM process (right)

The aim of the project is to contribute to the acceptance of AM technology by producing, certifying and flying a Flight Critical AM produced part. This raises the bar compared to non-flight critical parts, because of the more stringent regulations for Flight Critical parts.

In this project an existing conventional machined Flight Critical part will be replaced by a geometrical identical AM produced and certified part. Part substitution is not where the AM process has the greatest added value (see Figure 6), however it is the next step in acceptation of the AM technology.

The selected Flight Critical part for substitution is a Titanium Door Hinge, which is installed on a helicopter. This part will be created by the Laser Powder Bed Fusion (L-PBF) process, followed by heat treatment and machining operation. All surfaces will be machined, similarly to the substituted part, with the beneficial effect that the surface effects will be removed (particular the surface roughness improves). High Isostatic Pressure (HIP) treatment is a commonly applied process to reduce internal imperfections in AM produced parts. Because this is a costly process, the aim is to certify the part without using the HIP process.

The challenge of metal AM lies in the fact that the bulk material is created while building the part and one cannot rely on standard material properties established by the raw material supplier. The material properties need to be proven consistent because they depend on the feed stock material, the process parameters and the shape of the part.

Certification supported by test evidence is required to demonstrate that the Flight Critical part is airworthy. Generally 2 certification approaches can be distinguished:

1. Part certification
2. Process certification

Part certification is currently the common used approach to certify AM parts, because AM process standards are in development. Part certification requires the least effort compared to process certification.

The Flight Critical AM part will be certified against full strength requirements. Besides the static loads, the part is cyclically loaded, both in the 'low' cycle fatigue range ($N \approx 10^4$ -10^6) and in the 'high' cycle fatigue range ($N \approx 10^9$). To demonstrate the strength requirements, test specimens have been produced and are tested, see Figure 7. The manufacturing conditions of the specimens are equal to the to be substituted part (i.e. AM process parameters, heat treatment, machined surface, etc.).


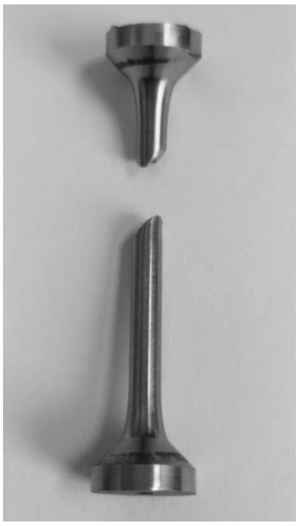

Figure 7 AM produced test specimens (left) and tested specimen (right)

The specimens are tested for both static and fatigue strength values. With the test results a mean S-N curve is generated to validate the 'low' cycle fatigue properties. These tests run up to $N = 10^7$ cycles. This curve is conservatively extrapolated to obtain the 'high' cycle fatigue properties at $N = 10^9$.

Relative large scatter in the fatigue properties is one of the challenges of the AM process, which is confirmed by the test results. Also the fact that the specimens have had no HIP treatment does not reduce the scatter. Therefore specific scatter factors have to be derived for the AM produced parts.

At the time of writing, the specimen testing is in progress. After completing specimen testing, the actual helicopter part will be produced and tested by cut-up testing and microstructure investigation. When this is successfully completed, the part can be certified.

AM is a promising production process since it offers low lead time, low material consumption and a high freedom of design. However, this project only targets to substitute a Flight Critical conventional machined part by a geometrical identical AM produced part. Nevertheless, the layer-by-layer build approach introduces many risks for errors on a microscale resulting in variation in material properties, particularly fatigue performance. This should be taken into account while designing a dynamically loaded part for AM. Therefore larger specific scatter factors for the AM produced part have to be taken into account. Furthermore the AM process should be improved reducing the errors like gas pores or lack-of-fusion to a level that it does not cause a larger variation in material properties compared to wrought or forged conditions.

2.6. Methodology for predicting the fatigue life of lug joints subjected to combined in-plane and out-of-plane loading

Rutger Kuijpers, René Alderliesten, TU Delft, Tim Janssen (GKN Fokker)

A structural joint type commonly applied in aeronautics is the lug joint, in which load is transferred via a pin. These joint types are used in aircraft for the attachments of flaps and ailerons (aircraft movables) to the wing. With the next-generation aircraft comes the use of new aircraft movable concepts, which compared to traditional lug joints also impose oblique- and out-of-plane loads. With the introduction of oblique and lateral (out-of-plane) loads on lugs - illustrated in Figure 8 (a) - the need arises for more detailed fatigue life prediction methods that take these load conditions into account.

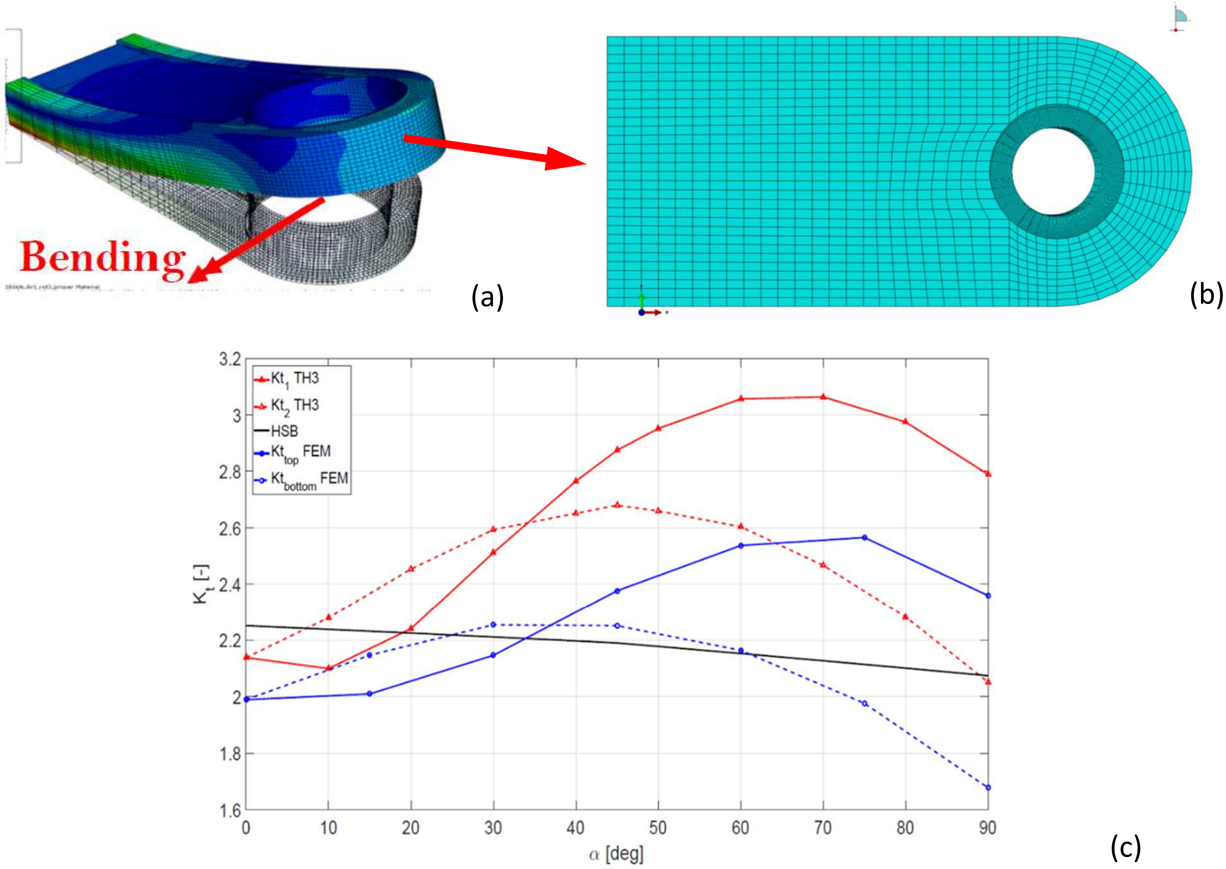

Figure 8 Illustration of a lug joint loaded in-plane and out-of-plane (a), FE-model for a straight lug with fine mesh in hole perimeter (b), and comparison between stress concentration factors obtained from FEA and two handbook solutions [7]

Hence, this study aimed at developing a methodology for predicting the fatigue life for lug joints subjected to combined in-plane and out-of-plane loading. The current fatigue prediction methods are all based on axially loaded lugs. In concept, these methods relate the nominal stress of an arbitrary lug to a reference lug through certain correction factors. To derive additional correction factors for oblique and out-of-plane load components, Finite Element Analyses (FEA) were performed on different loaded lugs using ABAQUS/CAE from SIMULIA by Dassault Systèmes. Both straight (Figure 8 (b)) and tapered lugs were simulated with and without lug hole eccentricity. Through simulating multiple cases of adding taper angle, load angle and lateral loads (out-of-plane component) and comparing these to the axial load conditions, an attempt was made to establish corrections factors to account for these load orientations previously not accounted for. In addition, it was observed that the lug hole eccentricity required a separate correction factor

The study resulted in a methodology for predicting the fatigue life for various in- and out-of-plane loaded lugs. Although the method could be reasonably verified, see Figure 8 (c), experiments need to be performed to validate the work and the proposed correction factors.

2.7. Stress Intensity Factor solution development

Frank Grooteman, Netherlands Aerospace Centre NLR

Funded by the European Space Agency ESA and in close collaboration with Southwest Research Institute (NASGRO software), NLR has developed several new Stress Intensity Factor (SIF) solutions for displacement-controlled crack geometries for NASGRO. These are:

- Through crack at plate center with quadratic displacement field (v8 - TC24)
- Corner Crack with bi-quadratic displacement field (v8 - CC20)
- Surface Crack with bi-quadratic displacement field (v9 – SC33)
- Through crack from an offset with quadratic displacement field (v9)

The geometries of the first two cases, TC24 and CC20, are shown below in Figure 9.

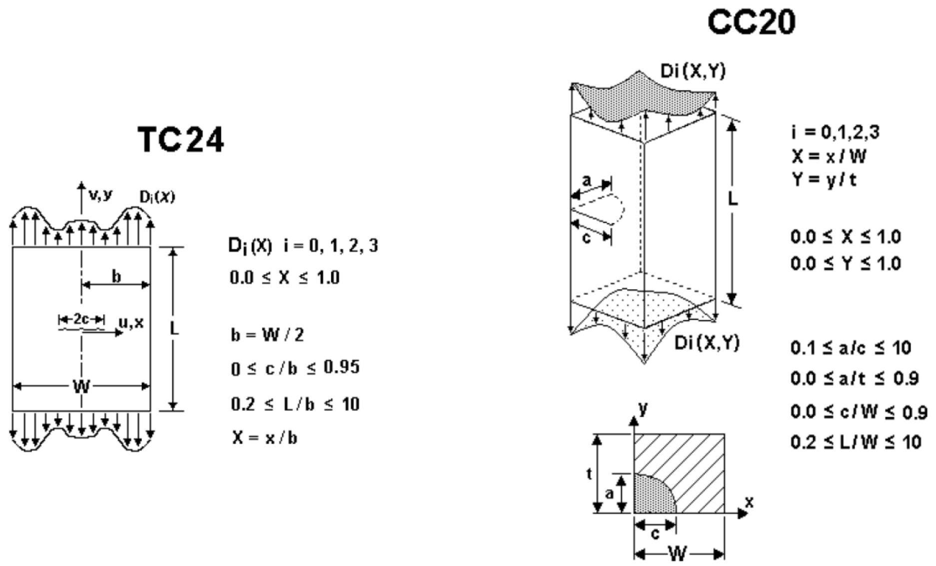

Figure 9 Examples of new displacement-controlled crack geometries in NASGRO.

Use was made of the finite element tool Abaqus, which offers a CAD modeller and an extensive application program interface with which external code can be written to modify the FE model and process the results. In a previous project at NLR, a generic framework was developed with which such stress intensity factor solutions can be generated much more efficiently for complex geometries and loads that formed the basis of these analyses. Automation is very important since many (tens of thousands) FE models needs to be generated and solved for the various crack geometries, especially 2D cracks, requiring a highly automated procedure to make this feasible.

Currently, a new solution is being developed for round notched bars with a semi-elliptical crack, see Figure 10, for which very limited SIF solutions exist in NASGRO.

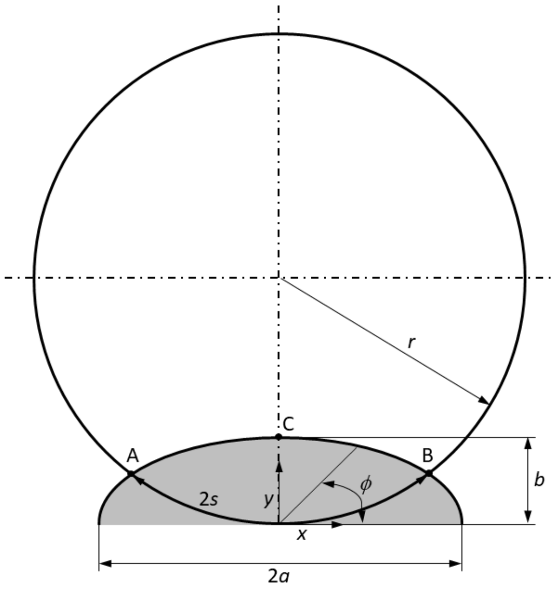

Figure 10 Semi-elliptical surface crack in a round bar.

2.8. Analysis of weight reduction of Al-Li high-altitude fuselage

J.E.A. Waleson, GKN Fokker

GKN Fokker manufactures bonded fuselage skin panels. Materials applied are 2024-T3 Clad for skins, 7075-T6 Clad for doublers and triplers, 7075-T73511 extrusions for stringers. The feasibility of a lighter Al-Li design with integrated doubler and bonded stringers was investigated for the skin panels. Both 2060-T8E30, which performs well for damage tolerance, and the more balanced 2198-T851 were analysed. Further, a comparison with 2425-T3 Clad was made. Because the thickness of the skin pockets is likely to have the largest effect on weight, the study focused on the criterion that was sizing for this thickness.

Analysis showed that the general buckling (Johnson-Euler) level was not critical for the skin pocket thickness and that the level could be increased by adding relatively little weight to only the bulb of the stringer in these panels, see Figure 11.

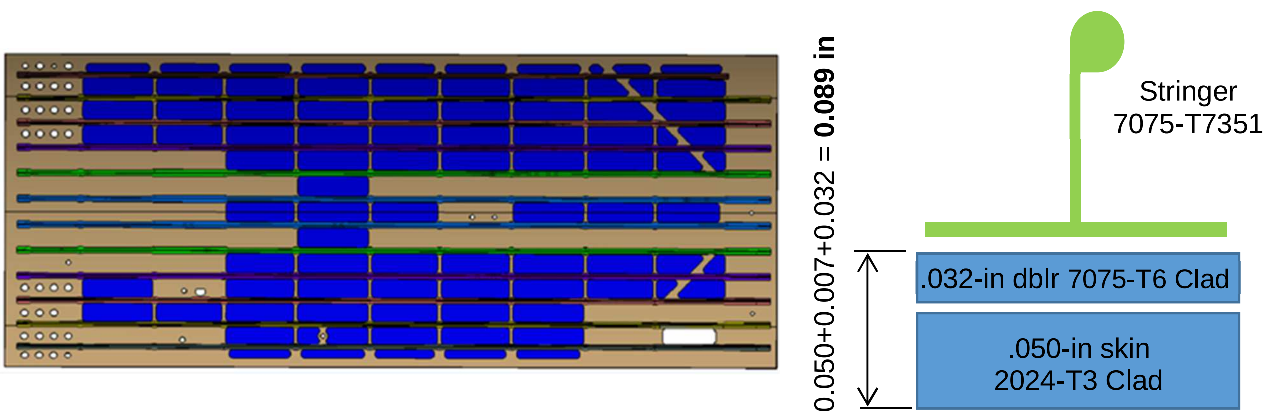

Figure 11 Fuselage panel with bulbed stringer section (right hand: cross section through stringer location).

In large areas of high altitude fuselages (altitudes above 45,000 ft) the sizing criterion was found to be the maximum acceptable cabin pressure loss or maximum pressure vessel opening for longitudinal cracks (with broken frame) after the required crack growth period [8].

The comparative analyses of the pressure vessel opening were limited to a mid-bay crack in .045-in skin pockets made of the new materials, because this type of analysis could be correlated with available test results for the .050-in 2024-T3 Clad baseline. It was assumed that a skin option which performance was sufficient for a mid-bay crack would also be feasible for a crack with broken frame. Complementing analyses of cracks centred about a severed frame were dropped because of budget limitations.

Da/dN data for the new considered alloys were available only at R=.1. Therefore, an equivalent number of cycles at equal ΔK, but with R=.1 was computed for the crack length and pressure vessel opening in .050-in 2024-T3 Clad, with which the number of cycles of the new alloys could be directly compared. Any different effect of the R-ratio on the alternative skin materials had to be neglected due to lack of data.

Analysis of pressure vessel opening

The pressure vessel opening of a mid-bay crack after growth during 4 intervals from a clearly detectable crack was used to compare the skin alloys. Both the crack growth rate and bending stiffness have an effect on the opening, which both were included in the analysis. To take advantage of better crack growth behaviour of the new alloys and the higher stiffness of the Al-Li alloys they were analysed with a smaller skin pocket thickness: .045 in compared to .050 in of the baseline 2024-T3 Clad.

The smaller thickness increases the normal stress, which has an effect on the rate and, hence, the length of the crack and the pressure vessel opening. Cracks that initiate along stringers tend to grow away from the stringer, which causes flapping of the skin, see Figure 12. The smaller thickness decreases the bending stiffness limiting the flapping, which also has a direct effect on the pressure vessel opening.

Before using the analysis for the assessment of the new alloys, it was validated with a test on a curved pressurized panel for the baseline material 2024-T3 Clad of .05-in thickness.

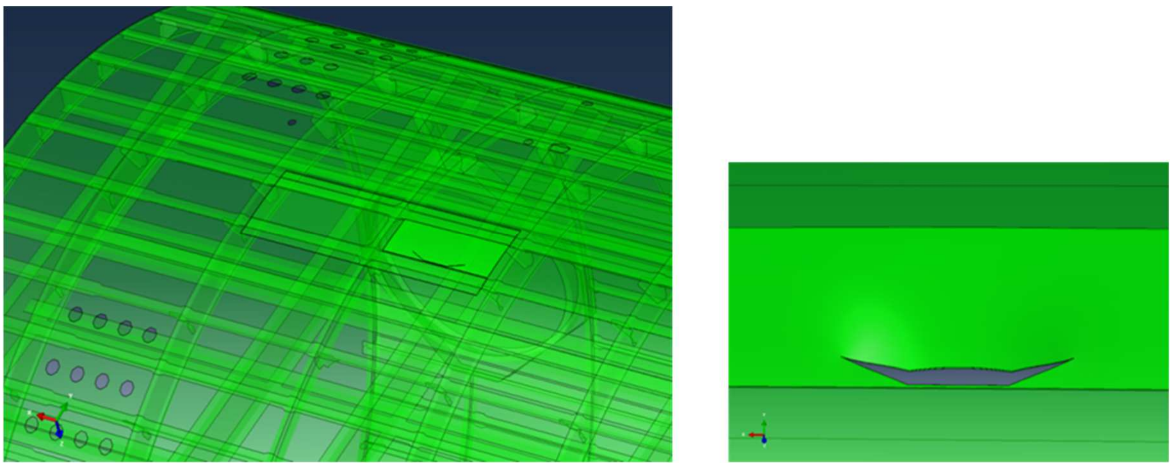

Figure 12 The FEM result that reproduces the crack along a stringer growing away from it and causing flapping of the skin.

The adopted analysis approach was developed by Vincent Bouwman from 4RealSim Services. In the area of the crack the skin is split in three layers of quadratic hex-elements:

- Outer layers of .0039 in (.10 mm) thick;
- Middle layer of .0421 in (1.07 mm) thick.

The crack tip is assumed one straight line through all layers, normal to the surface. A contour integral J on either side of the skin was computed in a geometrically non-linear ABAQUS Standard analysis, see Figure 13. The maximum J of both $J_{inner\ surface}$ and $J_{outer\ surface}$ was selected to compute the rate and crack angle. Assuming J equal to the strain energy release rate G, an equivalent mode-I stress intensity factor K_{eq} is calculated as a function of the crack length using:

$$J = \frac{K_{eq}^2}{E}$$

assuming a pure plane stress state for the .045 and .050-in skins. Note that for plane strain the resulting K_{eq} is a factor $1/(1-\nu^2)$ higher.

Further, the crack angle as function of its length was determined as the angle of the crack extension that yielded the largest difference in J (or strain energy). For the .045-in Al-Li and .050-in 2024-T3 Clad skin pockets different models were created to account for the effect of the stiffness on the stress distribution, the crack angle, and the bending. Note that the models depend on the stiffness of the material but were assumed independent of the da/dN curve. With this curve the growth rate was calculated using K_{eq}, from which the crack length as function of the number of cycles was determined.

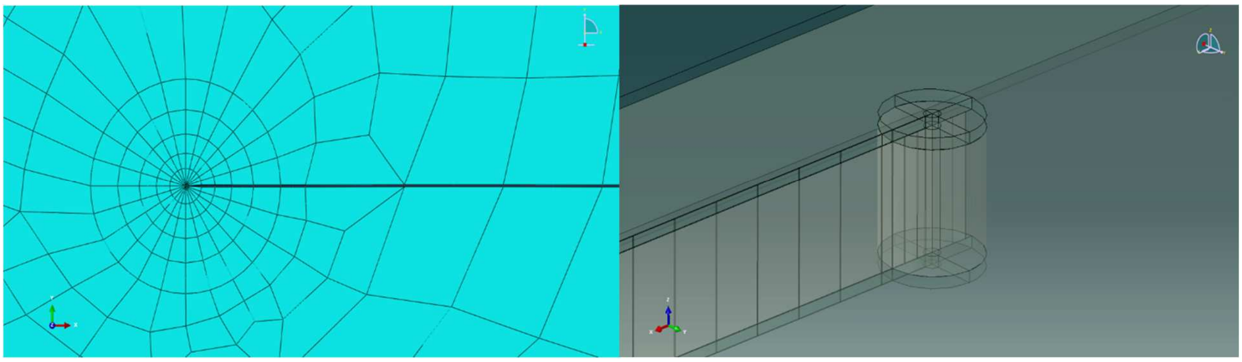

Figure 13 Meshing to compute contour integral J on either side of the skin.

Correlation of .050-in 2024-T3 Clad analysis with test

Input data and analyses with an effect on the final computation of the pressure vessel opening are:

- Far field stress distribution including skin pillowing, which was correlated to test;
- Computation of the J-integral including the effect of skin bending;
- Derivation of the equivalent mode-I ΔK;
- Da/dN data;
- Computation of the crack angle;
- Local bending of local crack edges.

Figure 14 shows the correlation of the *crack length* of the analysis with that of the test for .050-in 2024-T3 Clad at 11 psi pressure differential cycles (R=0). The overall correlation was deemed acceptable. Two details may not have been captured well:

- In the test the rate within in the first interval seems higher which may be explained by the neglected effect of K_{III} close to the stringer;
- The rate in the test shows a relatively sharp increase after four intervals.

However, it was assumed that these effects were similar for the different materials, enabling comparative analyses. The shape of the crack correlated well with the test.

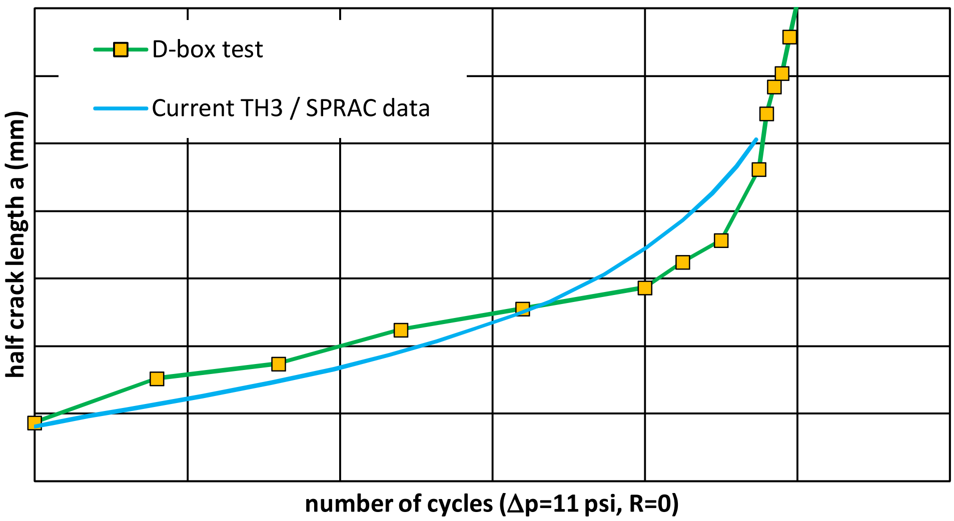

Figure 14 Correlation of computed crack growth in 2024-T3 based on "TH3/SPRAC" da/dN data with test data.

Crack growth results for new alloys

Fig. 5 shows the crack length and pressure vessel opening as a function of the number of Δp=11-psi cycles (using the available R=.1 da/dN curves) for .045-in skin pocket thickness of:

- 2198-T851;
- 2060-T8E30;
- 2524-T3 Clad.

The pressure vessel opening of mid-bay cracks after 4 intervals (R=0) were used to compare these new thinner materials to that of .050-in 2024-T3 Clad. For the actual comparison the crack length in .050-in 2024-T3 Clad at equal ΔK but R=.1 cycles is added as reference, e.g. 3.1 intervals at equal ΔK but R=.1 result in similar crack length and pressure vessel opening as after 4 intervals at R=0.

Analysis shows that a clearly detectable crack in a .045-in Al-Li 2060-T8E30 skin pocket reaches a similar pressure vessel opening as in the thicker, 050-in 2024-T3 Clad in a considerably longer interval than required. The interval is longer even when the da/dN curve at R=0 is used for 2024 and da/dN curve at the more critical R=.1 (equal ΔK) for 2060 as a conservative approach. This means that the assumption that the R effect is similar for both alloys needs not be used. This favourable result supported the argument for further research and testing of 2060-T8E30.

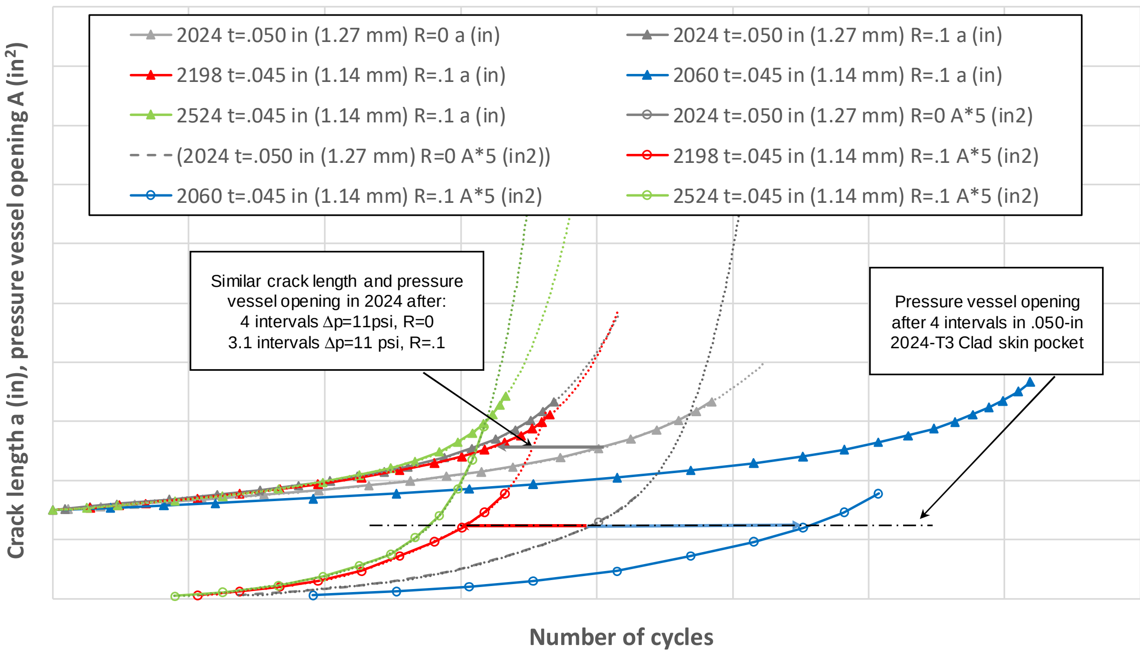

Figure 15 Crack length a and pressure vessel opening A as a function of the number of cycles for .045-in 2198-T851, 2060-T8E30, and 2524-T3 Clad. .050-in 2024-T3 Clad is added as baseline.

3. Adhesively Bonded Interfaces

3.1. The use of acoustic emission and composite peel tests to detect weak adhesion in composite structures

Sofia Teixeira de Freitas, Dimitrios Zarouchas, Hans Poulis, TU Delft

Adhesive bonding is one of the most promising joining technologies for composite aircraft. However, to comply with current aircraft certification rules, current safety-critical bonded joints, in which at least one of the interfaces requires additional surface preparation, are always used in combination with redundant mechanical fasteners, such as rivets and bolts. This lack of trust in bonded structures is mostly linked to the fear of lack of adhesion or a “weak bond”.

The aim of this study is to tackle this challenge by assessing the ability to use composite peel tests and acoustic emission (AE) technique to assess adhesion quality and distinguish a good bond quality from a “weak bond”.

Composite Bell Peel (CBP) tests and Double-Cantilever-Beam (DCB) tests were performed on contaminated and non-contaminated CFRP bonded specimens. The results show that peel strength drops significantly at the location of the contaminated interface that has led to weak adhesion, as a result from adhesive failure, see Figure 16. The AE signals obtained during DCB tests show different features for cracks growing at the interface (“weak bonds”) and inside the adhesive layer (cohesive failure), see Figure 17. In addition to this, scattering of the AE signals were observed in the contaminated specimens with “weak bonds” as illustrated in Figure 18. More information is provided in [9].

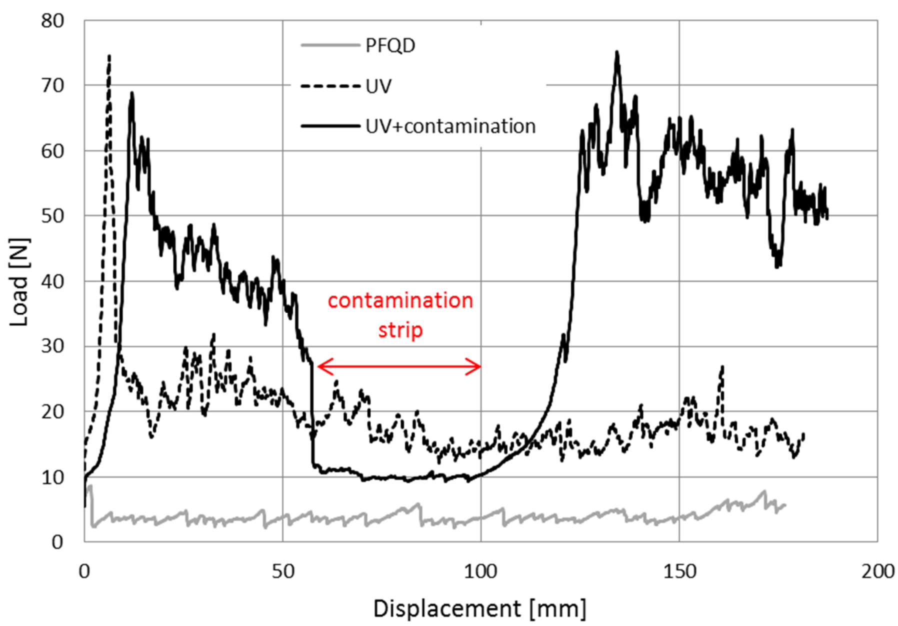

Figure 16 Representative load displacement graphs from the CBP tests.

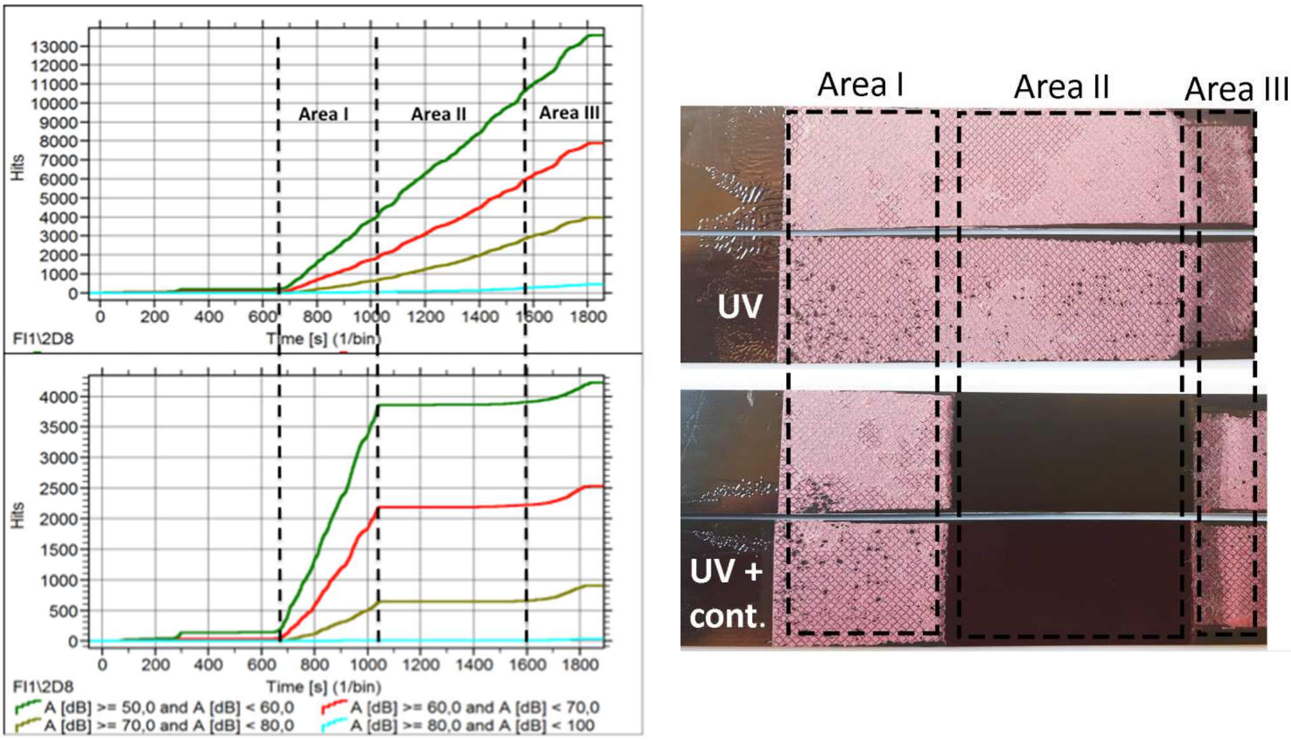

Figure 17   The cumulative number of hits during the tests for specimen without and with contamination respectively (Area II, lower specimens – contaminated)

	Non-contaminated specimen (UV)	Contaminated specimen (UV + cont.)
50-60 dB (*)	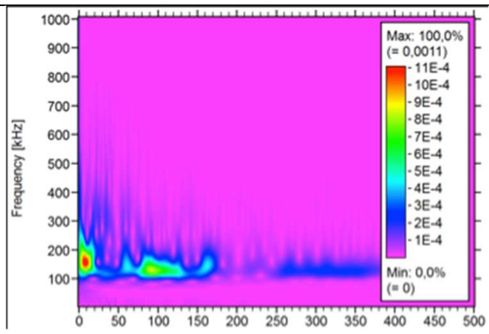	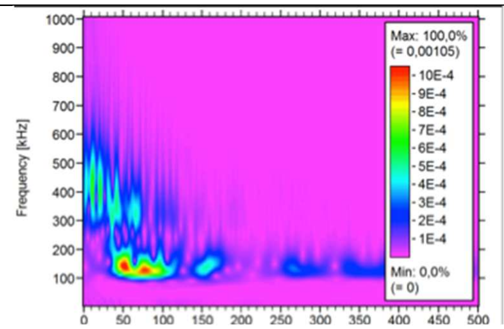

(*) peak amplitude range

Figure 18   The frequency time analysis of AE signals recorded during crack propagation of Area I (see Figure 2), from non-contaminated and contaminated specimens.

3.2. How pure mode I can be obtained in bi-material bonded DCB joints: a longitudinal strain-based criterion

Wandong Wang, Romina Lopes Fernandes, Sofia Teixeira De Freitas, Dimitrios Zarouchas, Rinze Benedictus, TU Delft

An essential question to predict the structural integrity of bi-material bonded joints is how to obtain their fracture properties under pure mode I. From open literature, it is found that the most commonly used design criterion to test mode I fracture is matching the flexural stiffness of the two adherents in a DCB coupon. However, the material asymmetry in such designed joints results in mode II fracture as well.

In this work, a new design criterion is proposed to obtain pure mode I fracture in adhesively bonded bi-material DCB joints by matching the longitudinal strain distributions of the two adherends at the bondline - longitudinal strain based criterion. A test program and Finite Element modelling have been carried out to verify the proposed design criterion using composite-metal bonded DCB joints – see Figure 19. Both the experimental and numerical results show that pure mode I can be achieved in bi-material joints designed with the proposed criterion – see Figure 20. G_{II}/G_{I} ratio is reduced by a factor of 5 when using the proposed longitudinal strain based criterion in comparison with the flexural stiffness based criterion – see Figure 21. More information is provided in [10].

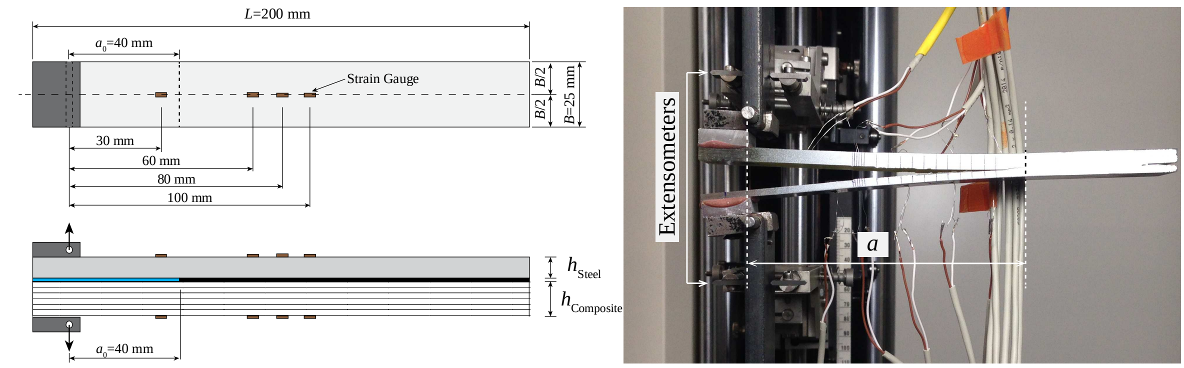

a) Specimen dimensions b) Test set-up

Figure 19 Composite-steel DCB specimens.

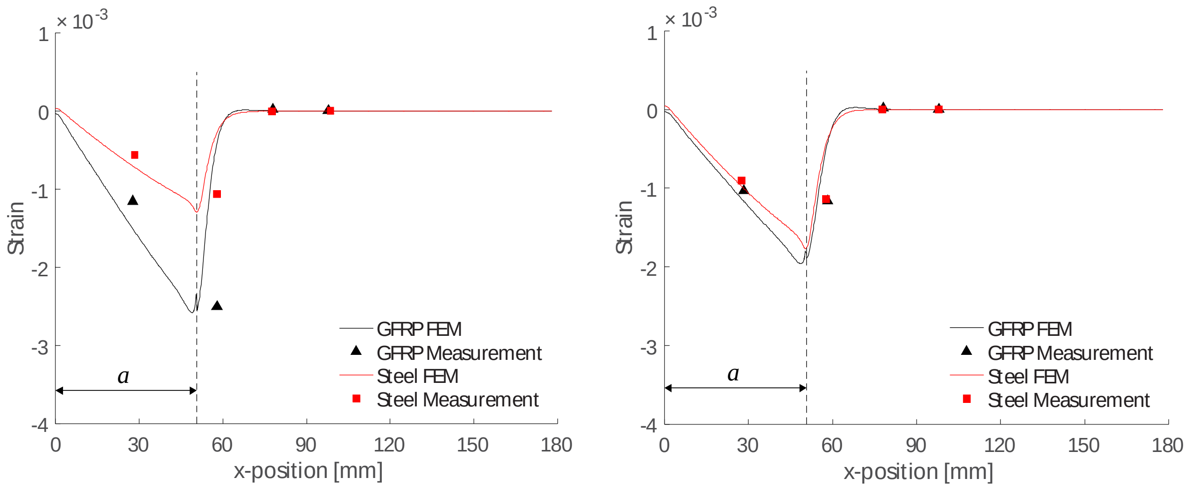

a)Curvature based criterion b)Strain based criterion

Figure 20 Longitudinal strains as a function of the x-position on the outer surfaces of both adherends. The x-position is defined from the load application point.

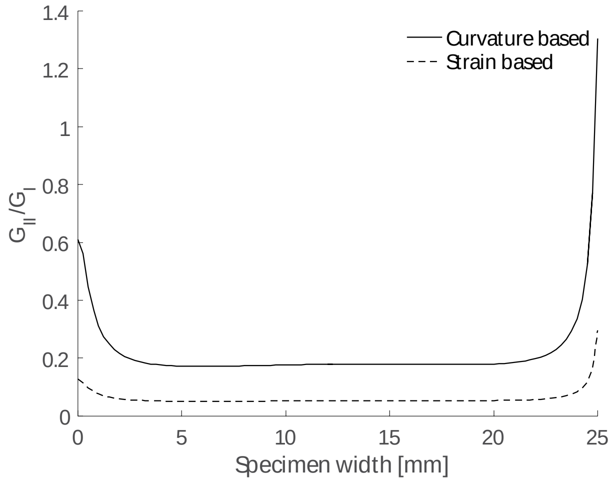

Figure 21 Comparison of the G_{II}/G_I ratio for both criteria: Strain based and Curvature based.

4. Composites & Fibre Metal Laminates

4.1. Determination of Mode I Fatigue Delamination Propagation in Unidirectional Fibre-Reinforced Polymer Composites

René Alderliesten (TU Delft), Andreas Brunner (empa)

To characterise mode-I (tensile opening) delamination behaviour of fibre reinforced polymer composites (CFRP), standard test methods are available for determining the quasi-static fracture toughness (ISO 15024) and the fatigue delamination onset (ASTM D 6115). These standard test methods, however, do not cover the fatigue delamination propagation behaviour, which is required for the purpose of design and reliability assessment. Development of standard test methods appropriate for determination of design values is hindered, because of the contribution of large-scale fibre bridging often observed in fatigue delamination testing of unidirectional laminates. The amount of fibre-bridging occurring in structural applications will depend on the laminate lay-up, but also, to some extent on the loading mode. For design, a "conservative" value is desirable, and hence, quantification of the effects of fibre-bridging on delamination propagation in unidirectional laminates would allow for estimating the intrinsic delamination resistance of this laminate. Together with consideration of the scatter, an intrinsic design limit can then be established, satisfying the safety factor requirements defined in design guidelines.

To this aim, a test procedure is in development within ESIS-TC4 describing the use of the Double Cantilever Beam (DCB) specimen in a tensile test machine capable of applying cyclic displacements of constant amplitude at a constant frequency in the range between 1 and 10 Hz. The procedure specifies an experimental procedure to quantify and exclude the contribution of large-scale fibre bridging in mode I fatigue fracture tests of unidirectionally fibre-reinforced plastic composites.

This test procedure comprises performing multiple sequences per specimen, to enable the derivation of a zero-bridging delamination resistance curve via regression through and translation of all data. This test procedure is a modification and extension of a former test procedure, but also incorporates an analysis based on a modified Hartman-Schijve equation for the determination of scatter in the fatigue fracture curves (essentially da/dN versus a "$\sqrt{\Delta G}$" related quantity instead of the "conventional" Paris-equation correlating da/dN with ΔK or ΔG). To demonstrate the repeatability and reproducibility of the test procedure, a round robin exercise is being prepared with participants of the ESIS-TC4 committee, but also other parties are invited to participate.

4.2. The effect of frequency on the fatigue delamination growth rate in composites

Aravind Premanand, René Alderliesten, TU Delft

In this study, the influence of test frequency on the mode-I fatigue delamination response of unidirectional CFRP was investigated. Tests on double cantilever beam specimens were carried out at various test frequencies ranging from 5 to 40 Hz. Fatigue can be seen as a material degradation process through which the applied work in the form of strain energy is dissipated into damage and other energy dissipation mechanisms. Hence, the experimental data were evaluated through energy principles. Both the crack growth and strain energy dissipation were averaged over multiple load cycles. Similar to taking the derivative of the crack growth curve for *da/dN*, *dU/dN* was calculated by taking the derivative of the applied strain energy at each crack length, see Figure 22. These averaged quantities, *dU/dN* and *da/dN* were then correlated following

$$\frac{dU}{dN} = \frac{dU}{da}\frac{da}{dN}$$

in which *dU/da* effectively represents the physical strain energy release rate G_{phys}, see Figure 23.

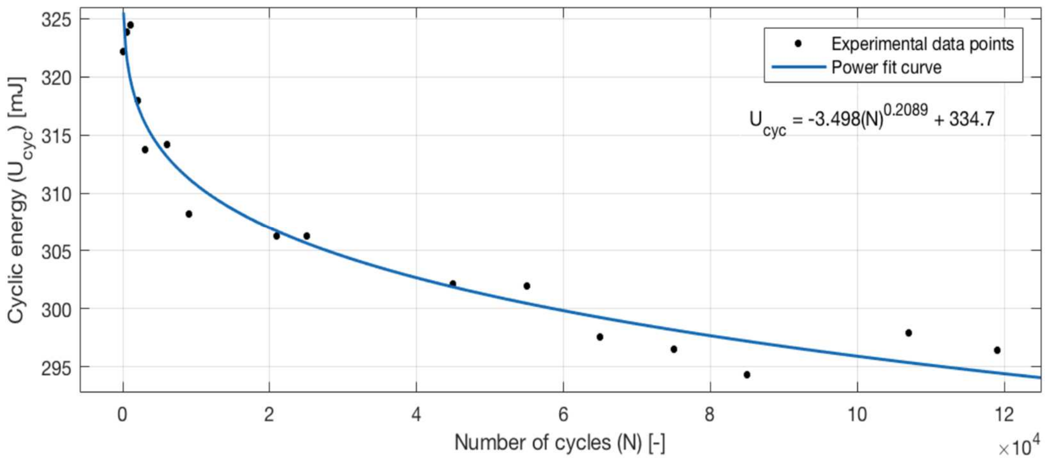

Figure 22 Cyclic strain energy data and power law fit against the number of cycles for 20 Hz test.

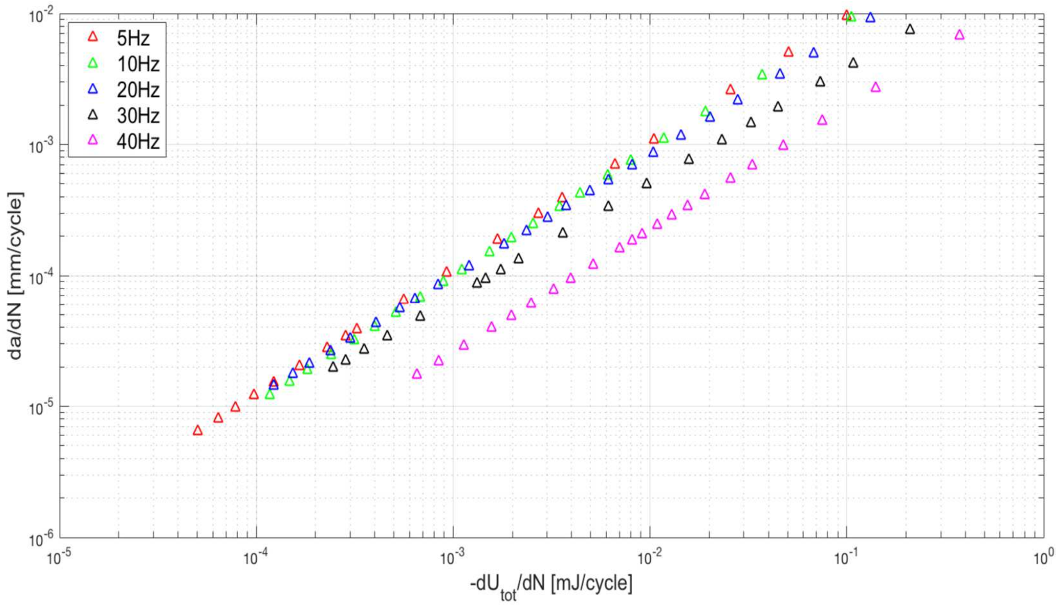

Figure 23 Influence of test frequency on the relationship between dU/dN and da/dN.

It was observed that at a frequency of 5Hz the load-displacement response was fairy linear, but that at higher frequencies the load-displacement response became nonlinear, exhibiting a stronger hysteresis. In case tests at all frequencies were analysed assuming a linear load-displacement response, no particular trend could be observed with respect to the test frequency. However, accounting for the non-linearity and hysteresis revealed a distinct frequency effect. Quantifying the hysteresis area as a measure for the dissipated energy in a load cycle, revealed that more energy is dissipated per unit crack increment at higher test frequencies. This means that at higher test frequencies the crack growth resistance G_{phys} is higher

Two possible mechanisms were investigated to explain this observed increase in G_{phys} with the increase in test frequency: Heat dissipation, and Internal heat generation

The latter would cause an increase in specimen temperature. Measurements from thermocouples and infrared camera demonstrated however, that no significant temperature rise occurred in the specimen during fatigue. Hence, the increase in hysteresis energy dissipation should be explained by rapid heat dissipation, through for example radiation, convection and conduction, or it should indicate another dissipative mechanism not yet identified.

Based on measurements and observations it is concluded that with increasing the test frequency, both the available energy *dU/dN* and the crack growth resistance G_{phys} increase. Depending on the interplay between these two parameters delamination growth may increase or decrease. It is recommended to study the relationship between strain rate (implicit in the test frequency), crack growth and strain energy dissipation mechanisms further, as full understanding of the relationships allow for accelerated fatigue testing. More information is provided in [11].

4.3. Investigating energy dissipation for a methodology with fatigue master curves

Sascha Stikkelorum, Dimitrios Zarouchas, René Alderliesten, TU Delft

Recent studies have identified a relation between damage growth and strain energy dissipation; the amount of energy dissipated during a load cycle is related to the damage extension. This relationship was the subject of this study with the objective to develop an analytical method for predicting fatigue life of composites under fatigue loading.

Constant amplitude fatigue experiments were performed in load control on open-hole specimens, shown in Figure 24, at various maximum load levels, a load ratio of 0.1, and a frequency of 5 Hz. Four lay-ups were studied: unidirectional (UD) laminates (0°), cross-ply (0°/90°), angle-ply (±45°), and quasi-isotropic (0°/90°/±45°), all manufactured with hand lay-up using Hexply 8552 prepreg tape.

Energy dissipates in three different forms: mechanical energy, heat and acoustic energy. The dissipated mechanical energy can be determined using the hysteresis area in the load-displacement curves. The heat can be minimised by testing at relative low frequencies and the acoustic energy can be measured using acoustic emission (AE). For the latter purpose all specimens were equipped with two AE sensors clamped at both ends of the specimen near the clamping area. During the tests, load and displacement data was measured by the test machine during an entire load cycle each 100th cycle. After each 100th load cycle pictures were taken by two cameras for digital image correlation (DIC). DIC was used to monitor the damage progression throughout the tests. Instead of testing until failure, specimens were tested until a number of cycles defined based on a damage threshold.

Typical damage mechanisms were observed such as splitting along the 0° fibres, transverse matrix cracks along the 90° and ±45° fibres, and interlaminar delaminations. The crack growth caused by fibre splitting in the 0°plies showed similar behaviour in the UD and cross-ply coupons, but not in the quasi-isotropic coupons where matrix cracking in the 90° and ±45° plies occurred first. The growth of the matrix crack in the 90° plies could not be recorded, as these cracks reached the coupon edge within the first 100 cycles.

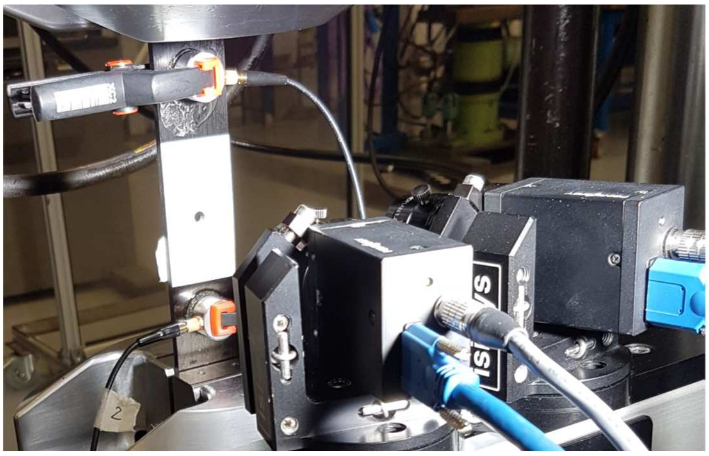

Figure 24 Picture of the test set-up. The upper acoustic emission sensor clamped to the specimen is for channel 1, while the bottom sensor is for channel 2

The recorded load and displacement data were used to calculate the cyclic work and the dissipated energy using the area underneath the load-displacement curves during loading and unloading. In UD, cross-ply and quasi-isotropic coupons the cyclic work first exhibited a steep increase, after which the slope decreased. For UD and cross-ply coupons this slope continued to decrease until an apparent asymptote was reached, while the cyclic work for quasi-isotropic coupons continues to increase over the number of cycles after the initial slope change. The cyclic work for the angle-ply coupons continued to increase with increasing number of cycles without a reduction in slope.

The dissipated energy per cycle was compared with the crack growth observed with DIC, however, no apparent correlation could yet be obtained. There appeared to be a linear relation between total cumulative amount of dissipated energy and number of cycles until failure, see Figure 25. Because the four lay-up configurations have different stiffnesses, the cyclic work for given load cycles are distinctively different. This cyclic work seemed to be related to the damage mechanisms observed.

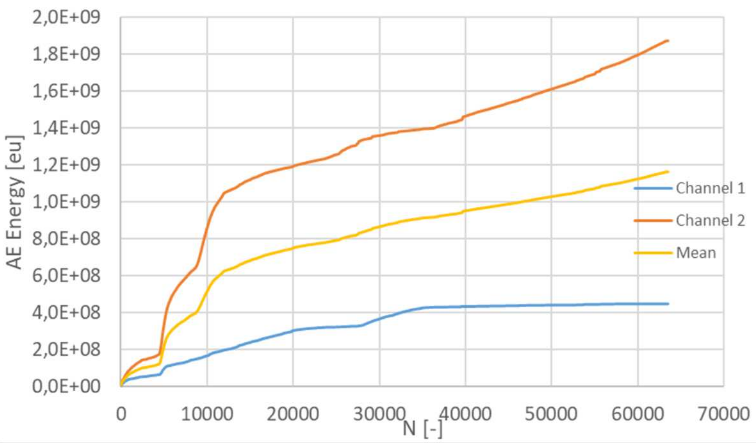

Figure 25 Cumulative acoustic emission energy versus amount of load cycles for UD coupon with maximum load of 53 kN and load ratio R = 0.1

The AE data was used to calculate the cumulative acoustic energy and number of acoustic hits. To see if acoustic features for different damage mechanisms could be identified, the registered rise time, duration and amplitude were plotted and divided based on the loads at which these hits were registered. This revealed that most of the damage growth occurred for loads between 75% and 100% of the maximum load, as illustrated in Figure 26. More information is provided in [12].

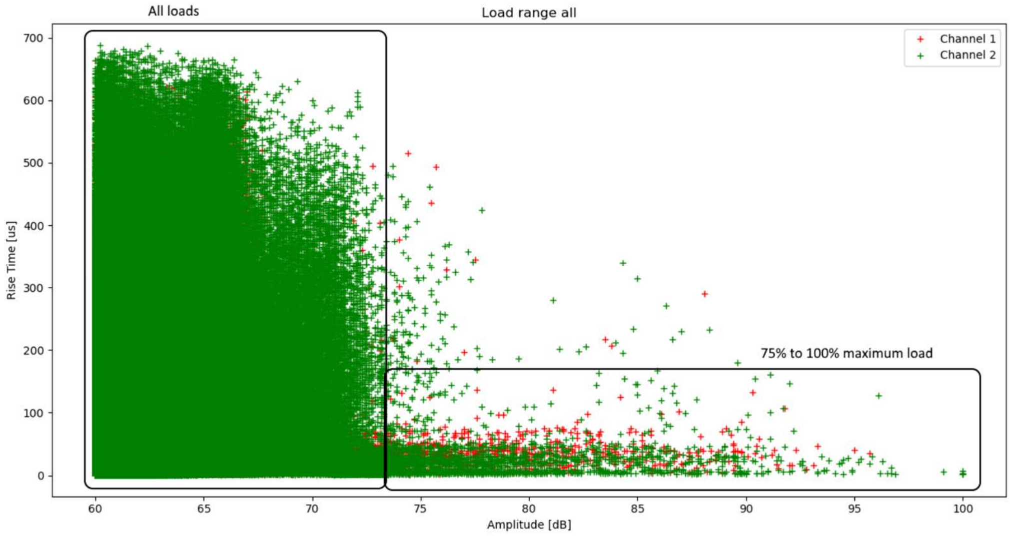

Figure 26   Rise time versus amplitude for UD coupon with maximum load of 53 kN and R = 0.1.

4.4. Towards the certification of bonded primary Fiber Metal Laminate structures by bolted Disbond Arrest Features

Ivar van Teeseling, Calvin Rans (TU Delft)

Nowadays, the widespread application of adhesively bonded joints in primary structures is challenged by the current certification regulations. One possible solution lies in the application of Disbond Arrest Features (DAFs) that prevent bondline damages from growing to a critical size.

The aim of this research is to study the working principles and potential risks of bolted DAFs in bonded Fiber Metal Laminates (FML)s by focusing on two elements;

1. Effect of reducing the Mode I Strain Energy Release Rate (SERR)
2. Relation between retardation/arrest of disbond growth and fatigue crack initiation in the FML adherends by the peak stress associated with the edge of the disbond

Fatigue experiments have been performed using Cracked Lap Shear (CLS) specimens with two different DAF configurations: (1) a bolted DAF and (2) a specially developed and produced clamped DAF which only affects Mode I. Additionally, a quasi-analytical model has been developed, verified, validated and used to expand on the experimental results.

It has been shown that reducing the Mode I SERR component is very effective mechanism in achieving the arrest of disbond growth (see Figure 1). Also, the arrest, or even retardation, of disbond growth can lead to the initiation of fatigue cracks in the FML adherends. The retardation/arrest of the disbond fixates this peak stress associated with the edge of the disbond at the same location leading to the local initiation of fatigue cracks.

An earlier study suggests that the initiation and growth of these fatigue cracks can be detrimental to the arresting capabilities of bolted DAFs. This means that the arrest of disbond growth could initiate fatigue cracks that result in the loss of the arrest of that same disbond. Future research is required to understand this potentially self-destructive mechanism.

The MSc thesis containing the results of this study can be downloaded from [13].

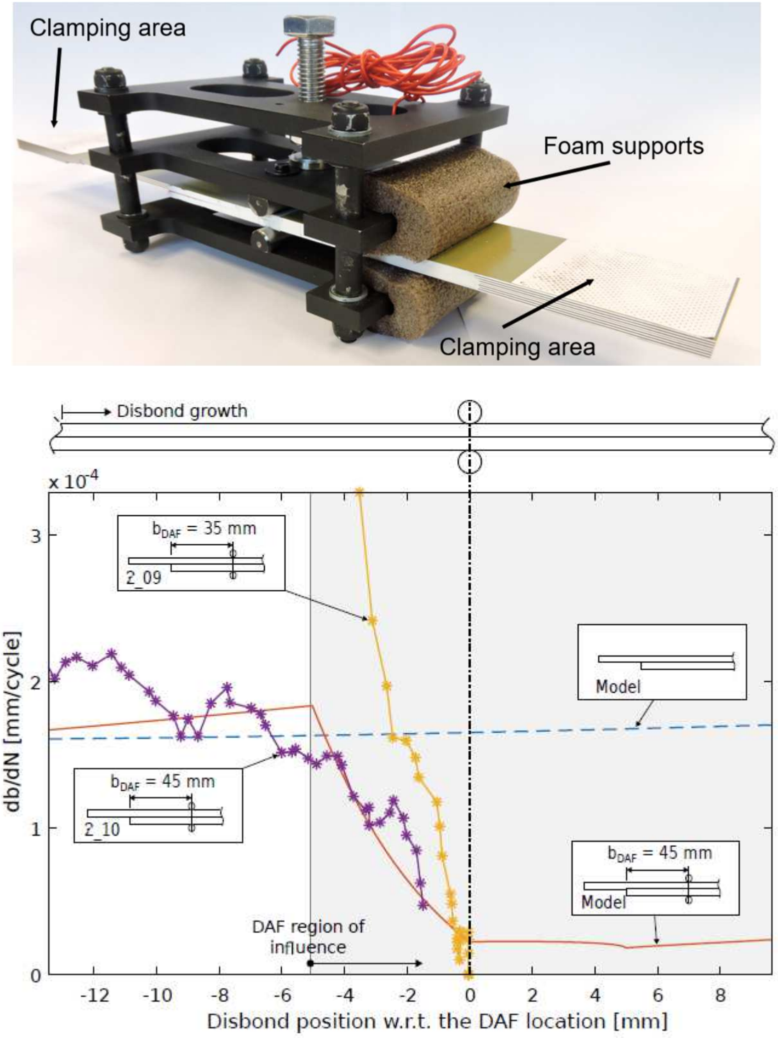

Figure 27 (db/dN) results of the clamped DAF. Experimental: (2_09) with DAF, (2_10) with DAF. Model: with and without DAF

4.5. No growth of butt joint damage in thermoplastic orthogrid fuselage panels

J.E.A. Waleson, J.W. van Ingen, S. van den Berg, GKN Fokker

In 2013, Fokker Aerostructures developed a new stiffened skin panel concept. The concept features frames that are welded to an orthogrid stiffening structure, thus eliminating a large number of mechanical fasteners. The concept is made possible by butt joining of stiffeners; stiffener plates are butt jointed to a skin laminate by melting them together [14].

A critical aspect for certification is showing no detrimental growth due to fatigue loads and sufficient residual strength of butt joint damages. Residual strength and onset of growth due to fatigue loads of a stringer-to-skin butt joint damage representing impact damage was tested on single stringer specimens loaded in compression, see Figure 28.

Onset of growth due to repeated loads appeared to require cycles well above 2/3 of the static failure load. Since the structure will be designed so that design ultimate load will not exceed static failure load, realistic fatigue cycles are expected not to cause damage growth.

Measured strains as function of the external load in the static test were correlated with an ABAQUS model with cohesive surface interaction to enable analysis of damage tolerance of fuselage panels. One of the correlations is illustrated in Figure 29. Testing on small panels is planned to assess the effect of adjacent intact stringers. Further, it is intended to establish a model for delamination growth due to fatigue loads.

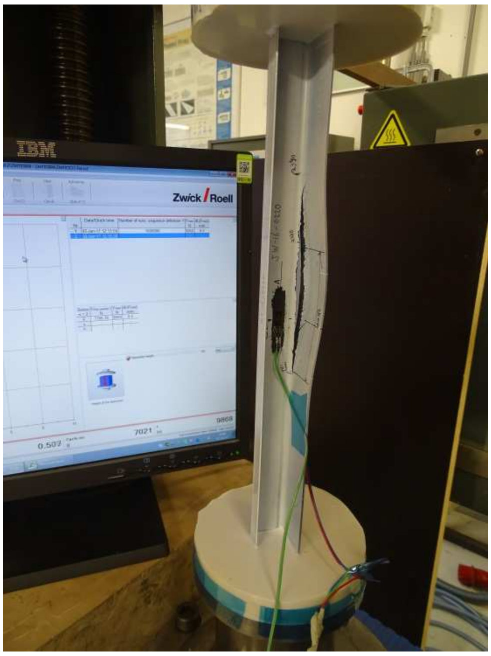

Figure 28 Fatigue testing of stringer-skin butt joint damage.

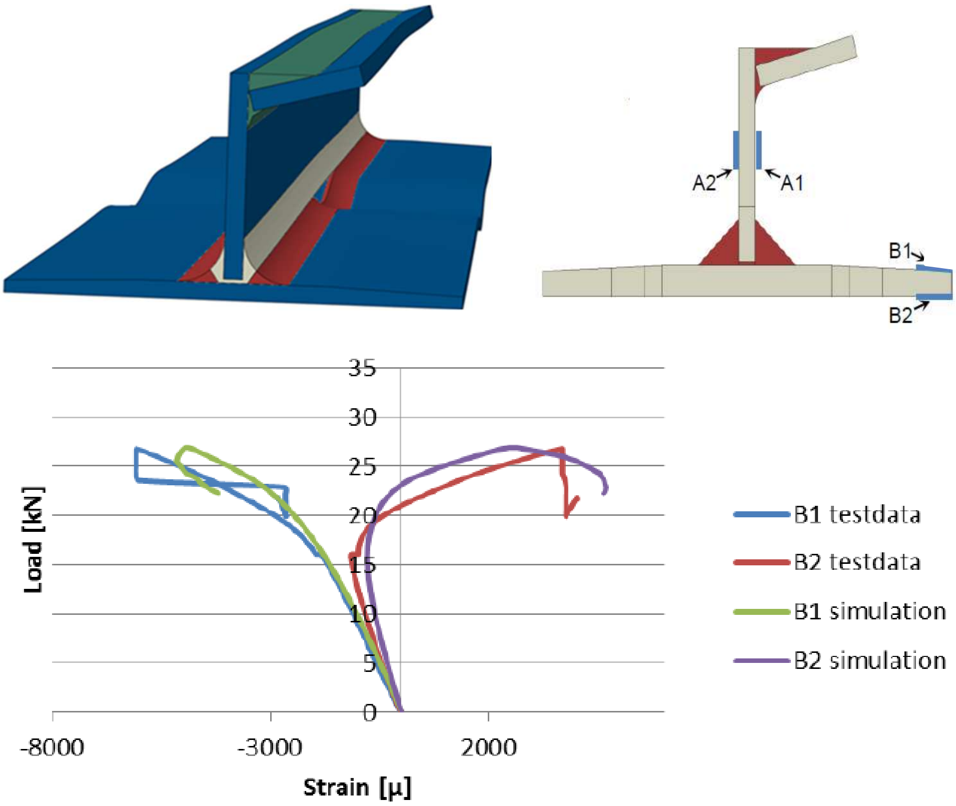

Figure 29 Correlation of predicted and measured strains as function of external static load.

5. Prognostics & Risk Analysis

5.1. Extreme Prognostics of Composite Structures

Nick Eleftheroglou, Dimitrios Zarouchas, René Alderliesten, Rinze Benedictus, TU Delft

Driven by advantages in structural efficiency, performance, versatility and cost, composite structures are increasingly applied in a variety of industries e.g. aerospace, wind energy, automotive. However, in spite of decades of application and research, the precise process of fatigue damage accumulation is still unknown and depends on several parameters such as the type of material and the lay-up, loading frequency and sequence and the form of the fatigue cycle. Additionally, the multi-phase nature of composites and the variation of defects, which cannot be controlled completely during the manufacturing process, result to a stochastic activation of the different failure mechanisms and make the fatigue damage analysis, and consequently the prediction of remaining useful life (RUL), very complex tasks. Probabilistic methodologies, combined with machine learning algorithms, have gained momentum the last decade and provide a platform for reliable predictions of RUL utilizing structural health monitoring (SHM) data. These data are needed in order to estimate the parameters of the selected RUL model since they are linked to the damage accumulation process.

It is worth mentioning that the fatigue life of a specific composite structure exhibits quite significant scatter, with specimens that either underperform or outperform. These specimens are often referred to as outliers and the prediction of their RUL is challenging because the training of the machine learning algorithm doesn't take into account data that are associated with their outlier performance.

This study presents a new RUL prediction model, the Extreme Non-Homogenous Hidden Semi Markov Model (ENHHSMM) which is an extension of the Non-Homogenous Hidden Semi Markov Model (NHHSMM). The ENHHSMM uses the available diagnostic measures, which are estimated based on the training data and adapts dynamically the trained parameters of the NHHSMM. As it was shown in previous studies, NHHSMM provided accurate RUL estimations of a non-outlier composite structure utilizing different SHM techniques such as acoustic emission (AE) [15] and digital image correlation [16], and it outperformed Bayesian Neural Networks [17], the state-of-the-art in data-driven approaches. Figure 30 illustrates the ENHHSMM, which consists of two parts; the training and testing process. The training process contains the training data and the stochastic model while the testing process uses the training process' output, the extracted testing data and dynamic diagnostic measures.

Fatigue experiments on open-hole composite specimens were performed in order to test the validity of the proposed RUL prediction model. The specimens, with stacking sequence $[0,\pm45,90]_{2s}$, were subjected to fatigue loading, R=0 and testing frequency of 10 Hz. AE technique was employed and recorded data which are related to the fatigue damage accumulation of the structure. The AE degradation histories of the seven open hole specimens are presented in Figure 31. Figure 32 presents the RUL estimations of the two available RUL prediction models regarding the left outlier, specimen05. Based on Figure 32 the ENHHSMM provides better outlier prognostics since the mean ENHHSMM RUL estimations are able to approach more satisfactorily the real RUL estimations than the NHHSMM. Additionally, the confidence intervals of the ENHHSMM contain the real RUL curve during almost the whole lifetime of specimen05 and their distance is shorter than the classic model. Furthermore, the initial mean 'extreme' RUL estimations almost overlaps to the real RUL and at the same time the 'classic' RUL estimations are not accurate, 150% overestimation. Therefore, the ENHHSMM can identify early enough an outlier and adapt the RUL estimations in an efficient and accurate way.

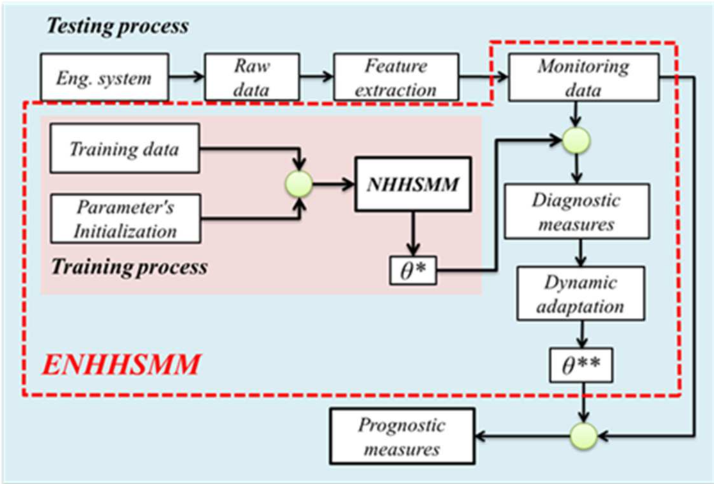

Figure 30 Flowchart of the new RUL prediction methodology

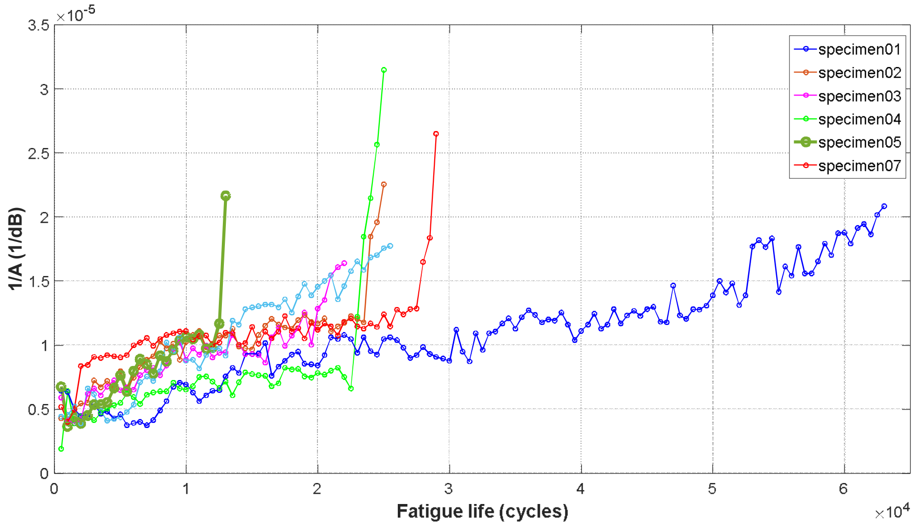

Figure 31 Acoustic Emission degradation histories.

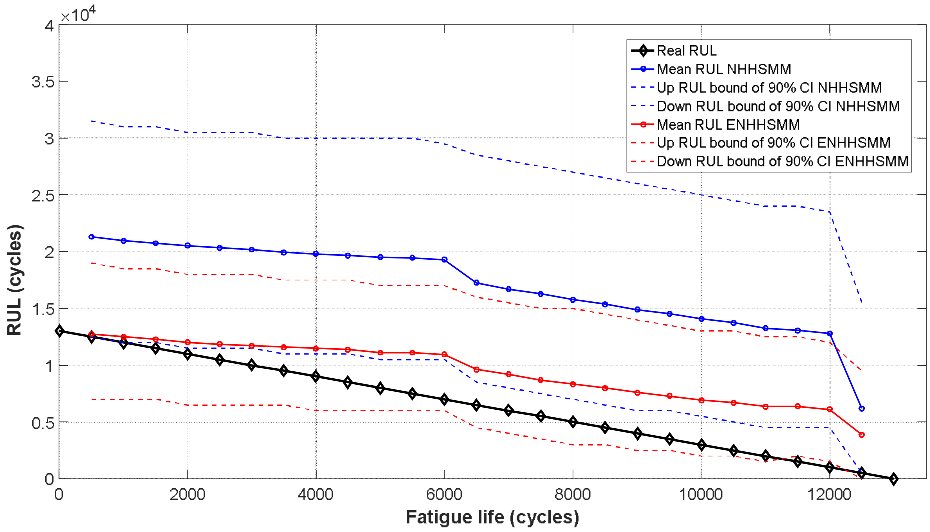

Figure 32 RUL estimations of the left outlier.

5.2. Structural risk assessment tool

Frank Grooteman, Netherlands Aerospace Centre NLR

The service life of a structure loaded by an alternating load shows considerable variability or scatter. This is mainly due to the variability in material properties, manufacturing quality (i.e. initial pre-crack size) and load history. The current design concept applied for aerospace structures is the deterministic damage tolerance philosophy, which includes the application of scatter and safety factors to the obtained crack growth life. In general, such analyses result in over-conservative life estimates and inspection intervals. The applied safety factors are quite arbitrary, but due to the built-in conservatism the current damage tolerance method has led to safe aircraft designs and continuing airworthiness. The probability of failure, however, cannot be calculated and the deterministic approach does not offer any means to balance the various risks and the mitigating means that are available in the sustainment phase of the aircraft.

Alternatively, a probabilistic damage tolerance analysis (structural risk analysis, SRA) can be performed, in which the variability of all important scatter sources is taken into account in a probabilistic manner. This requires the solution of a probabilistic problem. A tool for this is developed at NLR, called *SLAP* 'Stochastic Life APproach', see Figure 33.

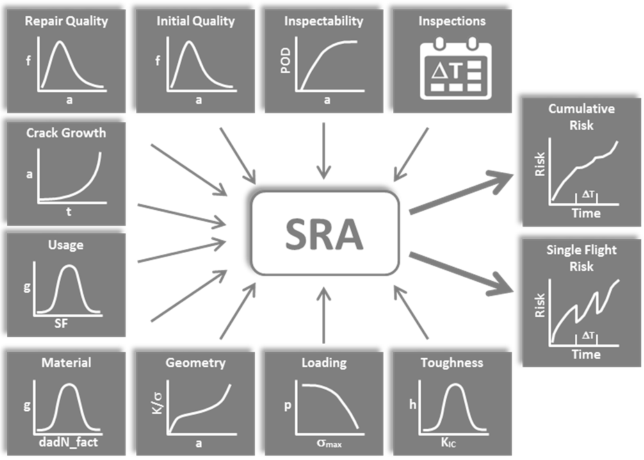

Figure 33 Schematized structural risk analysis.

For new military aircraft, SRA nowadays is mandatory and is prescribed in MIL-STD-1530D and MIL-STD-882E. In MIL-STD-1530D risk is defined in terms of the probability of failure for the next flight (hazard or single flight hour probability of failure, SFHPOF) and in MIL-STD-882E in terms of the cumulative probability of failure (POF) during the life of the aircraft. Structural risk analyses have become a valuable tool for fleet management, since it offers a risk (probability of failure) development over time of the fleet and each individual aircraft, which cannot be obtained from the traditional deterministic damage tolerance analysis. An example output of the risk level over time is given in Figure 34, in which the risk level is controlled by mandated inspections.

Contrary to other similar tools, the NLR SRA *SLAP* tool is able to take into account variation in material properties and loads, which both have a significant effect on the risk levels. Moreover, instead of using an equivalent initial flaw size (EIFS) distribution to predict crack growth from the start of service, an alternative is offered to start the analysis from the end of service life, i.e. from the failure distribution, for which a much more realistic distribution can be determined on service data contrary to the EIFS distribution.

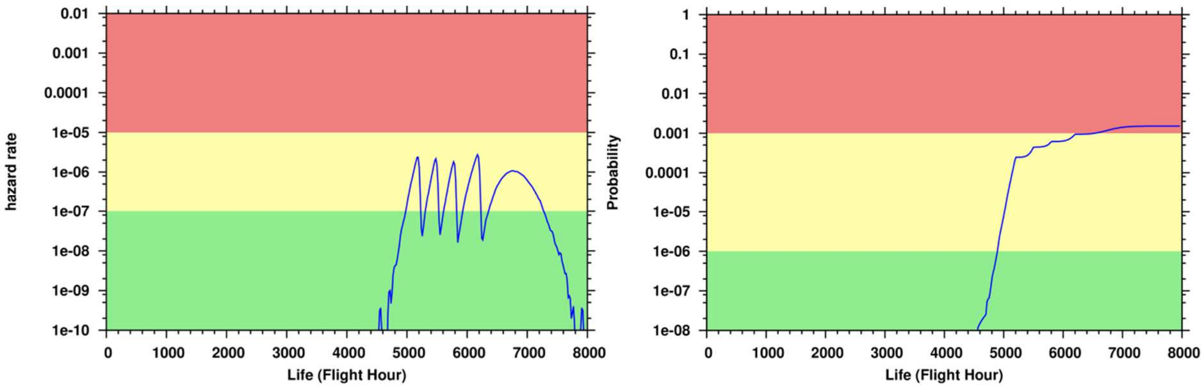

Figure 34 Example hazard (left) and cumulative probability of failure (right) plot

6. Non-Destructive Evaluation

6.1. NDI of hybrid structures

Jaap Heida, Netherlands Aerospace Centre NLR

The feasibility has been investigated of using Eddy Current (EC) inspection technology for the in-service detection of cracks in the metal substructure of hybrid structures with CFRP skins. For this purpose NLR has developed a modular reference component that consists of a scrap aluminium flap root rib and four interchangeable CFRP skin elements with different thicknesses, ranging from 4.75 mm to 19 mm. The skin elements are connected to the rib with 5 mm diameter NAS1580 fasteners. Both ferromagnetic and non-magnetic fasteners have been considered. The rib flange features three differently sized through-the-thickness EDM notches.

The hybrid reference component with artificial defects has been subjected to various EC methods, using both conventional probes (spot, sliding and ring) and an EC Array (ECA) module – see Figure 35. It was concluded that EC inspection of an aluminium substructure that is covered by a 19 mm CFRP skin is feasible. The best performance was demonstrated with the EC sliding probe, for both ferro and non-ferro fasteners. A practical EC test frequency for the investigated range of skin thicknesses is in the bracket between 500 Hz and 5 kHz. For the in-service inspection of large areas, the use of ECA is the preferred option, since it provides a 2-dimensional C-scan image in real time. However, its application has only been demonstrated for reference components with non-ferro fasteners and a skin thickness of 10-15 mm.

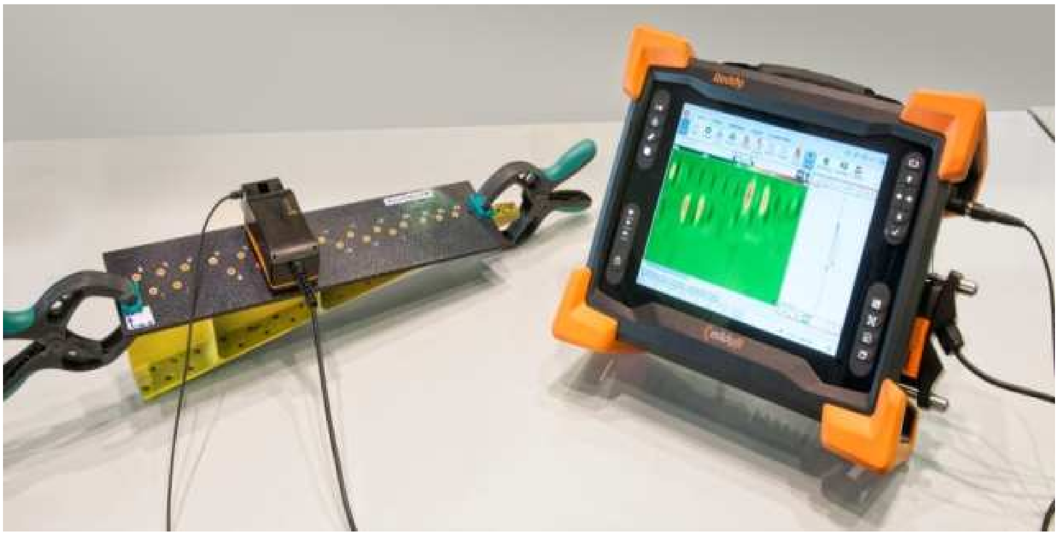

Figure 35 Eddy current array inspection of the hybrid reference component.

6.2. Characterisation of Matrix Cracks in Composite Materials Using Data from Fibre Bragg Grating Sensors

Aydin Rajabzadeh, Richard Heusdens, Richard C. Hendriks, Roger M. Groves, TU Delft

One of the most prevalent types of damage in composites is the formation of matrix cracks in the internal layers of composites, and detecting them has remained a challenge in the field of structural health monitoring. Due to the formation of cracks in the internal layers of composites, visual inspection is not possible, and other methods of inspection such as acoustic emission and ultrasonic inspection do not generally offer a high spatial resolution. Fibre optic-based sensors on the other hand, can be embedded between the layers of composites without severely changing the mechanical properties of the structure, and can provide information about the existence and the location of the cracks in real time. In this study, fibre Bragg grating type (FBG) sensors were used, which are manufactured by a refractive index modulation within the core of an optical fibre over a few millimetres to a few centimetres length. This length of anomaly acts as a partial reflector that reflects certain wavelengths of the input light to the optical fibre. The reflected spectrum of the FBG sensor is in fact the signal that contains the information about the transverse matrix cracks. Figure 36 (a) is a schematic design of the FBG sensor embedded between the composite layers and in contact with transverse matrix cracks, and Figure 36 (b) shows the calculated strain distribution along the FBG length, with peaks corresponding with the crack locations.

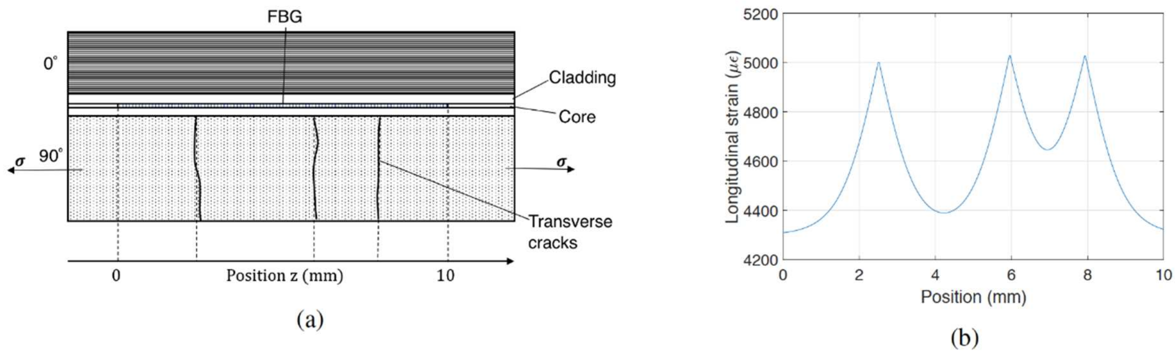

Figure 36 (a) A schematic of the formation of cracks in the proximity of an embedded FBG between layers of a composite panel, (b) The strain distribution along the length of the FBG, calculated using McCartney's theory for $\sigma = 400\ MPa$.

The FBG sensor, as shown in Figure 36, is sensitive to the cracks that form in its vicinity. Using a newly developed approximated transfer matrix model (ATMM), published in [18], an analytical closed-form expression was derived for the FBG reflection spectrum in contact with such strain field. It was then shown that taking the Fourier transform of this expression leads to distinct peaks at certain frequencies that correspond with the location of the cracks. For this it was necessary to first discretize the length of the FBG to a number of segments, say M. It was shown that the formation of cracks at segment i leads to the emergence of two peaks in the Fourier transform of the FBG reflection spectrum at angular frequencies $\omega = \{2i, 2M - 2i\}\ rad$. Also, for any two cracks at segments i and j, there will be a cross term in the Fourier transform at $= \{2i - 2j\} rad$.

The model was validated with experimental measurement from two different types of composite materials, carbon fibre reinforced plastic (CFRP) and glass fibre reinforced plastic (GFRP) with embedded FBG sensors, and the results agreed with our model. Figure 37 shows an example where a glass fiber specimen under a quasi-static tensile load was affected by two matrix cracks.

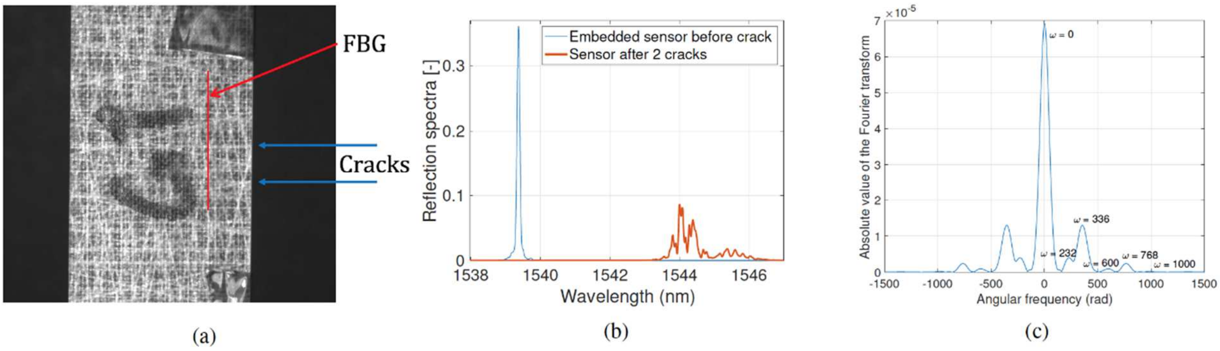

Figure 37 (a) GFRP specimen under a quasi-static tensile test, (b) Reflection spectra of the FBG before any cracks (blue) and after the formation of two crack (red), (c) Fourier transform of the windowed side-lobes of the reflected spectrum.

In modelling the FBG in this experiment, 500 segments were considered for the discretized FBG length, and at the location of the cracks, there were sudden changes of strain at segment numbers 300 and 384 of the FBG model. Therefore, according to the model there should be new peaks in the Fourier transform of the FBG reflection spectrum at $\omega = \{600, 768, 400, 232, 336\} rad$. In Figure 37 (c), it is illustrated that this prediction was correct. More information on this work is provided in [19].

6.3. Friction stir weldbonding defect inspection using phased array ultrasonic testing

Chirag Anand, Roger Groves (TUDelft), J. Fortunato, V. Infante (LAETE IDMEC), Daniel F.O. Braga, P.M.G.P. Moreira (INEGI, FEUP)

Weight reduction is an important driver of the aerospace industry, which encourages the development of lightweight joining techniques to substitute rivet joints. Friction stir welding (FSW) is a solid state process that enables the production of lighter joints with a small performance reduction compared to the base material properties. Increasing the FSW lap joint performance is an important concern. Friction stir weldbonding is a hybrid joining technology that combines FSW and adhesive bonding in order to increase the mechanical properties of FSW lap joints. FSW and hybrid lap joints were produced, using 2 mm thick AA6082-T6 plates and a 0.2 mm thick adhesive layer. Defect detection using non-destructive phased array ultrasonic testing (PAUT) has been made. Microscopic observations were performed in order to validate the PAUT results. Lap shear strength tests were carried out to quantify the joint's quality. PAUT inspection successfully detected non-welded specimens as shown in Figure 38, and correlated with macroscopic and microscopic analysis as shown in Figure 39, but PAUT was not able to distinguish specimens with major hook defects from specimens correctly weldbonded with small hook defects.

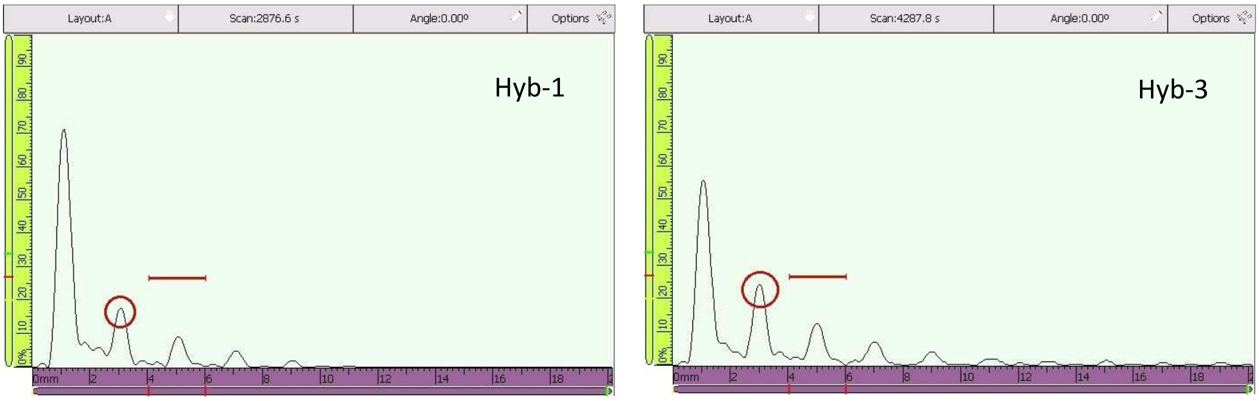

Figure 38   PAUT results obtained for hybrid specimens Hyb-1 and Hyb-3. The red circle signalizes the middle peak reflection from the adhesive layer. Vertical scale is wave amplitude in percentage, horizontal scale is distance

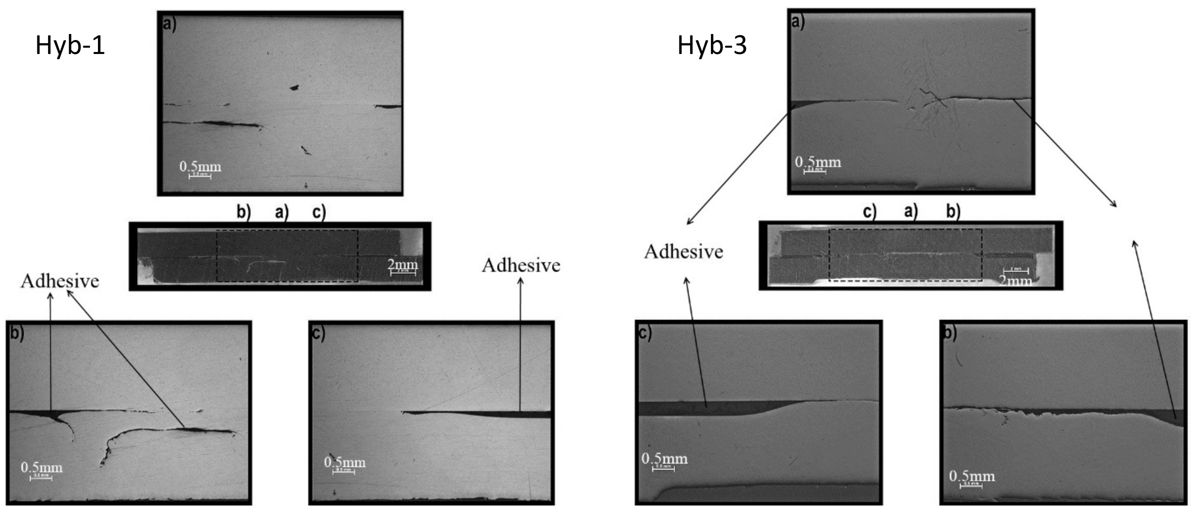

Figure 39   Macroscopic and microscopic figures of the Hyb-1 and Hyb-3 weld cross sections; a) centre of the weld, b) retreating side and c) advancing side.

6.4. Transducer Placement Option of Lamb Wave SHM System for Hotspot Damage Monitoring

Vincentius Ewald, Roger M Groves, Rinze Benedictus, TU Delft

Transducer placement strategies were investigated for detecting cracks in primary aircraft structures using ultrasonic Structural Health Monitoring (SHM). The approach developed is for an expected damage location based on fracture mechanics, for example fatigue crack growth in a high stress location.

To assess the performance of the developed approach, finite-element (FE) modelling of a damage tolerant aluminium fuselage has been performed by introducing an artificial crack at a rivet hole into the structural FE model and assessing its influence on the Lamb wave propagation, compared to a baseline measurement simulation. The efficient practical sensor position was determined from the largest change in area that is covered by reflected and missing wave scatter using an additive colour model. Blob detection algorithms were employed to determine the boundaries of this area and to calculate the blob centroid. The blob detection algorithm is based on the Laplacian of Gaussian with a kernel of 8-pixel connectivity. The Gaussian function G of an input image f(x,y) and feature scaling σ is given by

$$G(x,y,\sigma)=\frac{1}{\sqrt{2\pi\cdot\sigma^2}}\cdot\exp(-\frac{x^2+y^2}{\sigma^2})$$

while the Laplacian operator is given by

$$\nabla^2=\frac{\partial^2 f}{\partial x^2}+\frac{\partial^2 f}{\partial y^2}$$

By applying the Laplacian operator to the Gaussian function, one obtains the Laplacian of Gaussian, commonly known as LoG

$$\nabla^2 G(x,y)=\left(\frac{x^2+y^2-2\sigma^2}{\pi\cdot\sigma^4}\right)\cdot\exp(-\frac{x^2+y^2}{2\sigma^2})$$

The blob centroid $\hat{x}$, $\hat{y}$ with the scale $\hat{\sigma}$ is the simultaneously local extremum of the LoG in

$$(\hat{x},\hat{y},\hat{\sigma})=\arg\max\min_{(x,y,z)}(\nabla^2 G(x,y))$$

and this is the sensing location where the sensor should be placed.
An example for the merged differential image of captured Lamb wave propagation between 100 µs and 175 µs after being excited by the actuator is depicted in Figure 40, which depict residual Lamb waves due to perpendicular and angled (by 8°) cracks of 60 mm length that emerges from the middle rivet hole, respectively.

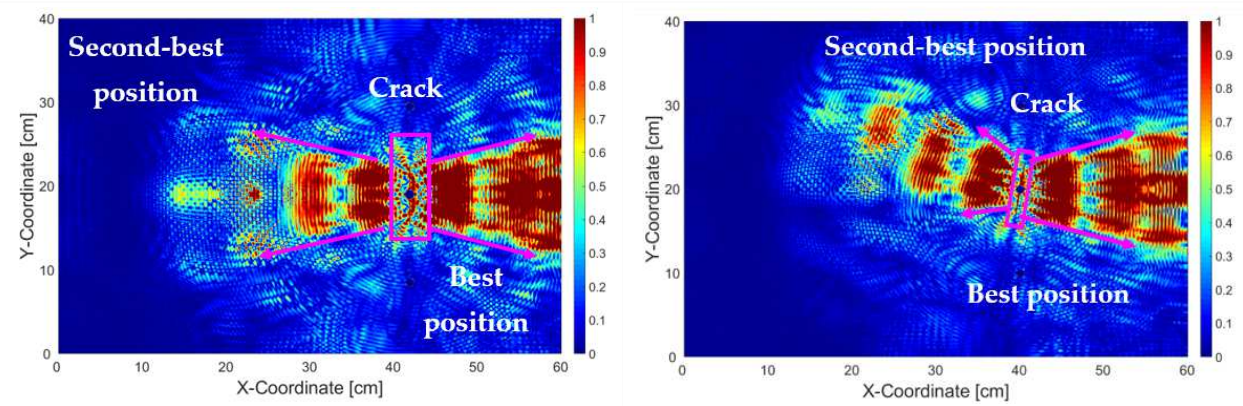

Figure 40 Differential image of Lamb wave propagation in a plate with 60 mm crack (left) and with angled 60 mm crack (right)

6.5. Fibre Optic Sensing for Structural Health Monitoring

Arjen Kloosterman, NLR

Fibre Optic Sensing (FOS) is a promising technique for the measurement of loads in aircraft structural components. However, despite the fact that FOS systems are already commercially available at reasonable costs, FOS is not yet widely used in the Structural Health Monitoring (SHM) of aircraft. An important reason is that the currently available systems are all stand-alone. This makes it very cumbersome to synchronize and correlate the FOS data to other in-flight measured parameters. To overcome this problem, NLR has teamed up with a supplier of a miniaturized FOS interrogator system and a supplier of flight test instrumentation hardware to develop a configurable prototype system that integrates FOS technology with an existing library of regular data acquisition modules. The objective is to demonstrate the simultaneous capability of the monitoring of loads & usage and the detection of structural damages & impact events. An additional component of the development program is the inclusion of the hi-speed contactless rotating power and data transfer module (CRPDT) that NLR is developing within the H2020 Clean Sky 2 framework for an airborne application on a civil tiltrotor. This eventually will enable FOS-based SHM of dynamic components. The CRPDT is able to transfer 140W of power and 1 Gbit/s of data over rotational joints that turn at rates up to 8,400 RPM.

The development program has started in 2018 and will finish in 2020. The result of the program will be the prototype of an integrated configurable FOS-based SHM system at a TRL of 7. It is expected that the industrial partners will further develop this system to a TRL of 9 and make it commercially available.

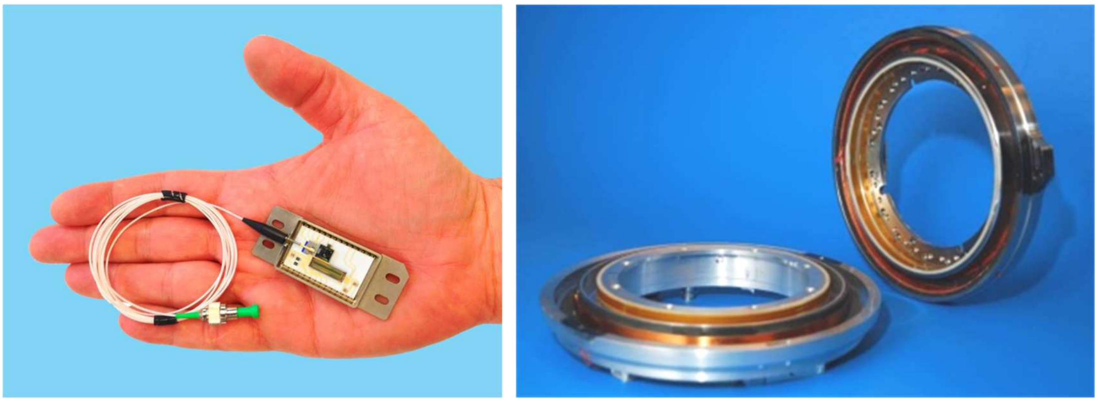

Figure 41 Miniaturized FOS interrogator system (left; courtesy Technobis) and contactless rotating power and data transfer module (right; NLR).

6.6. New damage indicators for structural health monitoring applications

Frank Grooteman, NLR

In the European project DEMETER, a joint project with DLR and Airbus, a new damage indicator is developed for damage monitoring in multiple load paths during flight. One of the concepts of the damage tolerance philosophy is the fail-safe concept, where the required residual strength of the remaining intact structure shall be maintained for a period of unrepaired usage through the use of multiple load paths or damage arrest features after a failure of a load path. The period of unrepaired usage necessary to achieve fail-safety must be long enough to ensure that the failure or partial failure will be detected visually and repaired prior to the failure of the remaining intact structure. Application of a reliable SHM system to detect the (partial) failure of the load paths would prevent periodic inspections and allow maintenance on demand after the system signals a (partial) failure. Especially in hard to inspect areas, for example the spars in a wing or connection of the tail plane to the fuselage, this could yield a significant maintenance cost saving. Moreover, it would allow a redesign of the structure; since any damage will be detected much earlier, the acceptable period of unrepaired usage may decrease, which will result in a lighter/cheaper structural design.

The damage indicator requires only one or a few strain sensors per load path. It has been validated in a test on a torsion box structure consisting of two similar aluminium (7075-T6) panels (400x820x2 mm) with 3 stiffeners each at a distance of 113 mm, as depicted in the figure below.

Three slots (175x25 mm) were inserted in the upper half of each panel in between the stiffeners to create three individual load paths. Optical fibre Bragg grating (FBG) strain sensors were applied as well as strain gauges for comparison. A load spectrum supplied by Airbus was applied to determine the robustness of the damage indicator for a realistic load spectrum and a climate chamber to examine the (in)sensitivity of the damage indicator to temperature variation.

The test was completed successfully and demonstrated the timely detection of a (partial) load path failure with fibre optic sensors and a suitable damage indicator.

Figure 42 SHM test bench at NLR with double stiffened panel in partially built up climate chamber

6.7. Experimental assessment of the influence of welding process parameters on Lamb wave transmission across ultrasonically welded thermoplastic composite joints

Pedro Ochôa, Irene F. Villegas, Roger M. Groves, TU Delft

Thermoplastic composite (TpC) joints produced by ultrasonic welding have a unique structure, with properties that are considerably different from adhesive bonds and are still not fully understood. Not only the bonding nature is different (molecular interdiffusion instead of adhesion), with unclear influence on the continuity of strain and stress across the overlap, but also the range of bond thicknesses is ten times smaller than in the case of adhesively bonded joints. Consequently, the interactions experienced by guided waves (GWs) in ultrasonically welded (UW) joints fall outside the domain of understanding obtained from previous research. Therefore, in this research the influence of ultrasonic welding travel on the transmission of GWs across UW TpC single lap-shear joints was investigated [20]. This study was the first step towards understanding the propagation of GWs in this new type of structural systems. Surface mounted piezoelectric transducers were used to test specimens welded with three different welding conditions, at two excitation frequencies, using the setup shown in Figure 43.

Two things were observed in the sensed GW signals acquired from the joints welded with a welding travel different from the reference travel. On the one hand, the energy transmission coefficient revealed only small amplitude variations with respect to the reference signals. On the other hand, the correlation coefficient showed that, despite the small amplitude variations, there were large signal shape changes with respect to the reference signals. These observations were attributed to a variation in the phase velocity of the GW modes in the overlap, without a significant change of their displacement mode shapes. This affected the phase lag between the GW modes in the overlap and, consequently, the reverberation pattern inside the overlap. As a result, the modification of the interference between the reverberated wave packets and the directly transmitted wave packets was dominated by signal shape changes.

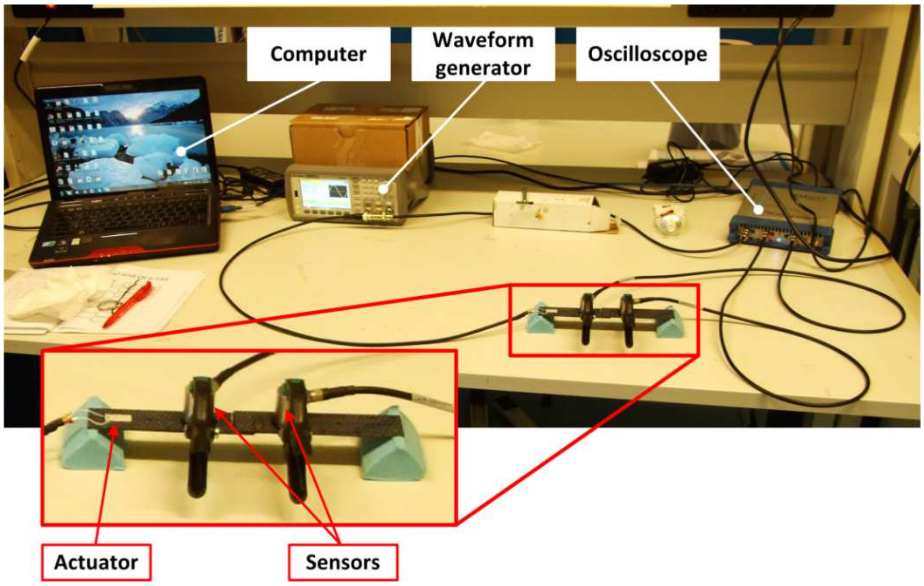

Figure 43. Setup used for the GW tests.

A correlation between the GW signal observations and the molecular interdiffusion across the weld interface was established by benchmarking the weld interface reflection magnitude for the different welding travel batches, obtained through ultrasonic phased-array B-scans (see Figure 44). The larger the welding travel, the more continuous the weld interface, and thus the stronger the molecular interdiffusion across the weld interface.

This study showed that GWs are sensitive to manufacturing-related variations that can occur in TpC UW joints, and it put forward a possible approach for detecting those variations. The acquired knowledge represents an important step towards the development of ultrasonic health monitoring capabilities for modern TpC aircraft structures. In turn, SHM systems are expected to contribute to the optimisation of maintenance programmes by providing information about when and where repairs are necessary.

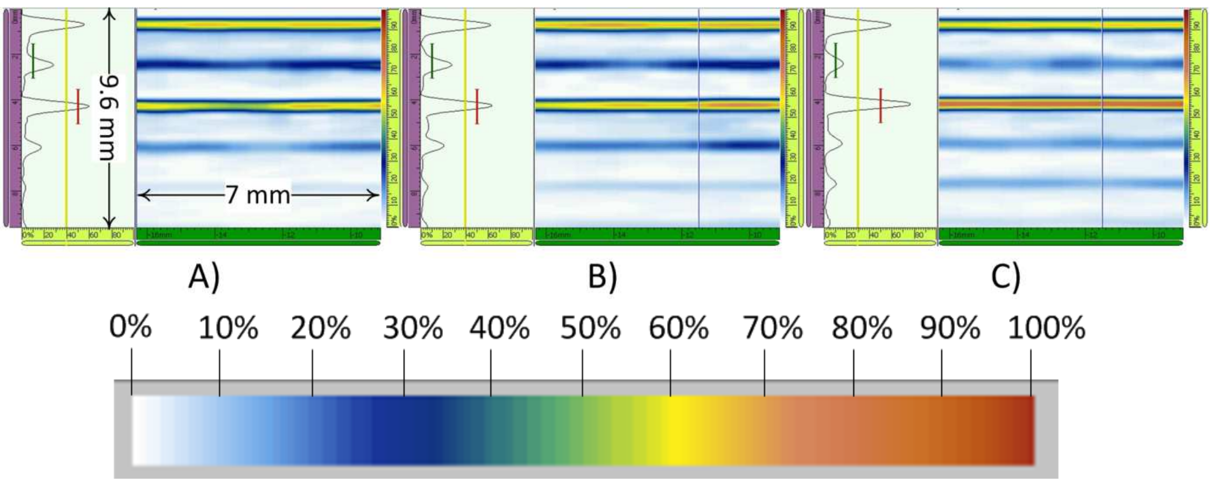

Figure 44. A- and B-scans from 5 MHz phased-array inspections of a representative specimen produced with a welding travel of a) 0.02 mm, b) 0.08 mm, and c) 0.12 mm. The A-scan percentage scale matches the B-scan colour scale (the closer to red, the stronger the reflection; the closer to white, the weaker the reflection). It is possible to see that the reflection from the welding interface gets weaker as the welding travel increases.

7. Structural Health & Usage Monitoring

7.1. Landing gear health monitoring

Frank Grooteman, NLR

Together with Meggitt, Technobis and Airbus, NLR is partner in the European project ALGeSMo on Advanced Landing Gear Sensing & Monitoring. In this project a system is developed for the measurement of the landing gear service loads, based on fibre optic sensing. The work consists in developing and testing landing gear loads measurement technology, in view of further functional integration with aircraft avionics, flight management and health monitoring systems. In addition to health monitoring of the landing gear, the system can also be applied for accurate and rapid classification of hard landing and overload events, to determine braking moments, for automated and accurate weight on wheels and centre-of-gravity position measurements, and for sensitive detection of air-ground transitions. One of NLR tasks is to develop a test rig in which the SHM system will be comprehensively tested.

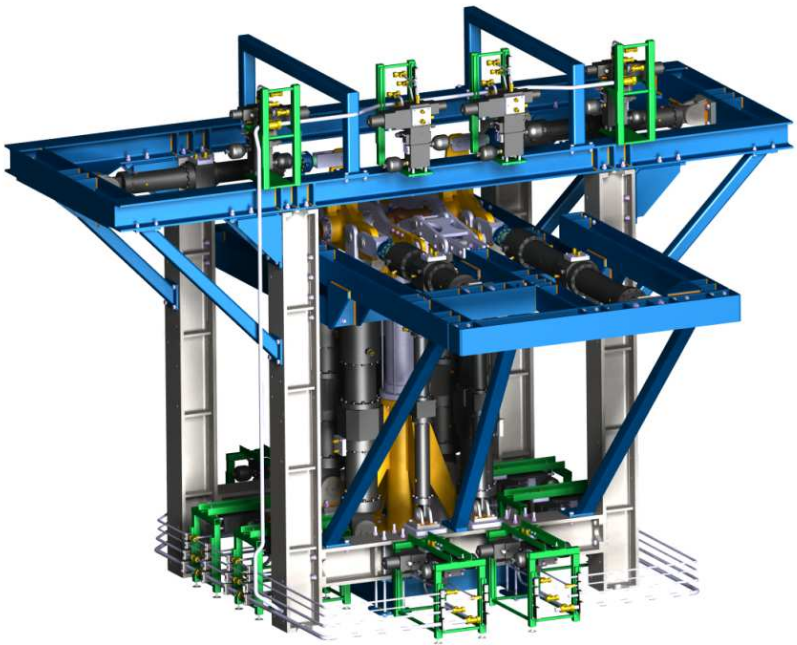

Figure 45 Landing gear health monitoring test bench at NLR.

8. Fleet Life Management

8.1. Individual tracking of RNLAF aircraft

Marcel Bos, NLR

The Royal Netherlands Air Force (RNLAF) and NLR collaboratively keep track of the loads and usage of most aircraft types in the RNLAF inventory, viz. the F-16 Block 15, C-130H/H-30, NH90, AH-64D, ICH-47D and ICH-47F.

This is done on an individual basis (individual aircraft tracking, IAT) and involves the installation of data acquisition and recording equipment, the development of databases and processing software, the development of fatigue and/or corrosion damage indices, the collection and processing of loads and usage data and the reporting of the processed data to the RNLAF. The results are used to:

- keep track of the consumed fatigue life;
- assess the severity of specific missions and mission types;
- evaluate and possibly optimize the usage of the fleets;
- optimize maintenance programs;
- assess/anticipate required structural modifications programs;
- provide the OEM with high-quality data in case of modification programs;
- rationalise decisions regarding tail number selection in the case of out-of-area deployment, fleet downsizing, decommissioning, etc.;
- develop load spectra for full-scale component testing;
- gain insight in the root causes of accidents and failures;
- enhance reliability analyses.

Details of these programs were already supplied in previous National Reviews. New activities involve the modernization of the data information systems and the fusion of the collected usage data with the maintenance databases of the RNLAF to enable and enhance reliability analyse efforts.

Figure 46 RNLAF aircraft types that are routinely tracked.

9. Special Category

9.1. Fatigue Crack Growth Failure and Lifing Analyses for Metallic Aircraft Structures and Components

Russell Wanhill (NLR), Simon Barter, Loris Molent (DST-G)

In 2016 Springer has published a so-called Springer Brief with the title Fatigue Crack Growth Failure and Lifing Analyses for Metallic Aircraft Structures and Components [21]. Springer Briefs are concise booklets that focus on a single topic.

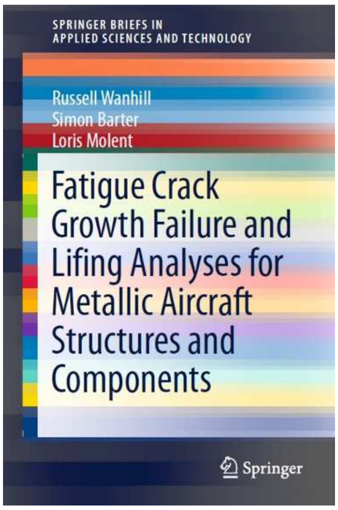

This book provides a concise discussion of fatigue crack growth (FCG) failure and lifing analysis methods for metallic aircraft structures and components. After a reasonably concise historical review, surveys are made of (i) the importance of fatigue for aircraft structural failures and the sources of fatigue nucleation and cracking, (ii) contemporary FCG lifing methods, and (iii) the quantitative fractography (QF) required for determining the actual FCG behaviour. These surveys are followed by the main part of the book, which is a discussion, using case histories, of the applicabilities of linear elastic fracture mechanics (LEFM) and non-LEFM methods for analysing service fatigue failures and full- and sub-scale test results. This discussion is derived primarily from the experiences of the Defence Science and Technology Group in Melbourne, Australia, and the Netherlands Aerospace Centre, Marknesse, the Netherlands.
The opinions expressed in this book are those of the authors and do not necessarily represent those of the organisations with which they are, or have been, associated.

References

[1] Van Kuijk J, Alderliesten RC, Benedictus R. *Fatigue crack surface area and crack front length: new ways to look at fatigue crack growth* MATEC Web of Conferences. 2018;165:13009 DOI 10.1051/matecconf/201816513009.

[2] Iost A., Lesages J. *On the existence of a pivot point for stage II fatigue crack growth* Eng Fract Mech. 1990; 36(4):585-596.

[3] Amsterdam E. *On the validity of the Paris equation*. Proceedings 17th Australian Aerospace Congress, 26-28 February 2017, Melbourne

[4] Amsterdam E, Nawijn M. *Fatigue tests for alloys*. Aerospace Testing International showcase 2018; 16-20.

[5] Smith KV. *Application of the dissipated energy criterion to predict fatigue crack growth of Type 304 stainless steel following a tensile overload*[J]. Eng Fract Mech. 2011; 78(18): 3183-3195.

[6] Quan H, Alderliesten RC, Benedictus R. *The stress ratio effect on plastic dissipation during fatigue crack growth* MATEC Web of Conferences. 2018;165:13002 DOI 10.1051/matecconf/201816513002.

[7] Kuijpers RC. *Methodology for Prediction of the Fatigue Life for Lug Joints Subjected to Combined In-Plane and Out-of-Plane Loading*, MSc thesis, Delft University of Technology, 2018 https://repository.tudelft.nl/islandora/object/uuid%3A3be70155-068a-4f41-8397-2a0bb71db5d3?collection=education

[8] AC 25-20, Pressurization, Ventilation and Oxygen Systems Assessment for Subsonic Flight including High Altitude Operation.

[9] Teixeira de Freitas S, Zarouchas D, Poulis JA. *The use of acoustic emission and composite peel tests to detect weak adhesion in composite structures*, The Journal of Adhesion. 2018: 743-766 DOI: 10.1080/00218464.2017.1396975

[10] Wang W, Lopes Fernandes R, Teixeira De Freitas S, Zarouchas D, Benedictus R. *How pure mode I can be obtained in bi-material bonded DCB joints: A longitudinal strain-based criterion*, Compos Part B. 2018; 153: 137-148. https://doi.org/10.1016/j.compositesb.2018.07.033

[11] Premanand A. *A study on the effect of frequency in delamination of CFRP*, MSc thesis, Delft University of Technology, 2017 https://repository.tudelft.nl/islandora/object/uuid%3A3be70155-068a-4f41-8397-2a0bb71db5d3?collection=education

[12] Stikkelorum S. *Investigating energy dissipation for a methodology to fatigue master curves*, MSc thesis, Delft University of Technology, 2019 https://repository.tudelft.nl/islandora/object/uuid%3A7cf54af6-ac94-439f-8c29-25cae8861637?collection=education

[13] Teeseling I van. *Towards the Certification of Bonded Primary Fiber Metal Laminate Structures by Bolted Disbond Arrest Features*, MSc thesis, Delft University of Technology, 2019 https://repository.tudelft.nl/islandora/object/uuid%3A85b6685a-52c8-4f0f-b05d-9752384a9c1c?collection=education

[14] Van Ingen JW. Thermoplastic Orthogrid Fuselage Shell, Sampe Journal. 2016; 52(5): 7-15.

[15] Eleftheroglou N, Loutas TH. *Fatigue damage diagnostics and prognostics of composites utilizing structural health monitoring data and stochastic processes.* J. Struct. Health Monit.2016; 15(4):473-488.

[16] Eleftheroglou N, Zarouchas DS, Loutas TH, Alderliesten RC, Benedictus R. *Online remaining fatigue life prognosis for composite materials based on strain data and stochastic modelling.* J Key Eng Mat. 2016; 713:34-37.

[17] Loutas TH, Eleftheroglou N, Zarouchas DS. *A data-driven probabilistic framework towards the in-situ prognostics of fatigue life of composites based on acoustic emission data*. J Compos Struct 2017; 161:522-5

[18] Rajabzadeh A, Heusdens R, Hendriks RC, Groves RM. *Calculation of the mean strain of smooth non-uniform strain fields using conventional FBG sensors*. J Lightwave Technol 2018; 36(17), 3716-3725.

[19] Rajabzadeh A, Heusdens R, Hendriks RC, Groves RM. *Analysis of the Side-lobes of FBG Reflection Spectra from Matrix Cracks in Composites. In Optical Fiber Sensors* (p. TuE97). Optical Society of America 2018.

[20] Ochôa P, Fernandez Villegas I, Groves RM, Benedictus R. *Experimental assessment of the influence of welding process parameters on Lamb wave transmission across ultrasonically welded thermoplastic composite joints*. Mechanical Systems and Signal Processing 2018; 99: 197-218.

[21] Wanhill R, Barter S, Molent L. *Fatigue Crack Growth Failure and Lifing Analyses for Metallic Aircraft Structures and Components*, Springer Brief, Springer Netherlands, 2018.